energies

MDPI

Review

Advancements in Manufacturing of High-Performance Perovskite Solar Cells and Modules Using Printing Technologies

Shohreh Soltani and Dawen Li *

Department of Electrical and Computer Engineering, The University of Alabama, Tuscaloosa, AL 35487, USA
* Correspondence: dawenl@eng.ua.edu

Abstract: Perovskite photovoltaic technology carries immense opportunity for the solar industries because of its remarkable efficiency and prospect for cost-effective production. However, the successful deployment of perovskite solar modules (PSMs) in the solar market necessitates tackling stability-based obstacles, scalability, and environmental considerations. This paper unveils a comprehensive examination of the cutting-edge advancements in the manufacturing of perovskite solar cells (PSCs) and modules, with an emphasis on high-speed, large-area printing. The paper underscores the substantial progress achieved in printed PSCs and PSMs, demonstrating promising electrical performance and long-term device durability. This review paper categorizes printing techniques compatible with large-area high-speed manufacturing into three distinct families: blade coating, slot die coating, and screen printing, as these common printing practices offer precise control, scalability, cost-effectiveness, high resolution, and efficient material usage. Additionally, this paper presents an in-depth investigation and comparison of superior PSCs and PSMs fabricated by printing on power conversion efficiency (PCE), stability, and scalability.

Keywords: perovskite-based solar cells and modules; industry-compatible printing processes; screen printing; slot die coating; blade coating

Citation: Soltani, S.; Li, D. Advancements in Manufacturing of High-Performance Perovskite Solar Cells and Modules Using Printing Technologies. *Energies* **2024**, *17*, 6344. https://doi.org/10.3390/en17246344

Academic Editor: Hyunwoong Seo

Received: 9 October 2024
Revised: 6 November 2024
Accepted: 11 November 2024
Published: 17 December 2024

1. Introduction

Perovskite-based photovoltaic cells have gained increasing recognition as an emerging class of high-efficiency and cost-effective futuristic photovoltaics used to benefit human being and address climate change. The performance of single-junction perovskite solar cells (PSCs) has witnessed a remarkable boost from 3.8% to 26.7% since the initial perovskite photovoltaic device was reported in 2009 [1]. This substantial improvement indicates the prospect of perovskite-based photovoltaics to battle with traditional and mature gallium arsenide (GaAs), silicon, and cadmium telluride (CdTe) thin-film solar cells. Recent advancements in trap manipulation at the charge transporting layer/perovskite (CTL/PVSK) interface and device structural optimization have further demonstrated the great capability of perovskite-based photovoltaics to achieve higher efficiency and stability [2–5]. The key component of perovskite energy cells is the perovskite light absorbing and charge generating layer, which possesses exceptional optoelectronic properties, encompassing a durable carrier diffusion length [6], high light absorption capability [7], tunable band gap [8], and weak exciton binding energy [9]. While initial research on perovskite-based solar cells focused on tiny-scale laboratory units, currently, significant efforts are being made to develop superior large-area perovskite-based solar modules (PSMs) [10,11]. These PSMs hold potential for applications in outdoor large-scale power production and serving as indoor power delivery component. Additionally, there is anticipation for future upgrades within the domain of portable wearable electronics, targeting the development of low temperature processed pliable PSCs based on flexible substrates as an optimistic addition of rigid cells [12]. However, the widespread adoption of PSMs in industrial power generation is thwarted by their short lifespan and lack of low-cost and reliable techniques

for large-scale manufacturing [13]. Currently PSCs and PSMs can be prepared using either roll-to-roll (R2R) or sheet-to-sheet (S2S) processing methods. Among these, R2R processing, which is well-suited for high-volume manufacturing of printed electronic units, is considered a more efficient approach to produce solution-processable solar cells because of its high production throughput and simplified configuration [14].

Among the various solution printing techniques, screen printing, slot die coating, and blade coating are particularly well-suited to producing perovskite-based photovoltaics. Slot die coating is a continuous and high-throughput method that affords meticulous control over the thickness uniformity of the printed films. It is highly desirable to large-scale production and facilitates efficient material utilization. Screen printing is a versatile and cost-effective technique that enables the perovskite inks to be printed over expansive areas. It offers exemplary pattern resolution and can be readily merged into R2R processing. Along with its relative simplicity and cost-effectiveness, blade coating endows exceptional control over film quality and thickness, rendering it ideal for both laboratory-scale research and small-scale production. These printing techniques demonstrate significant developments in terms of throughput, scalability, cost-effectiveness, and deposition quality control, thereby positioning them as highly promising selections for the manufacturing of perovskite-based solar cells and modules [15–17]. In the subsequent sections of this review paper, these coating approaches will be further examined, and several illustrative examples will be assessed to demonstrate their practical usage and effectiveness in the synthesis of functional films in perovskite solar devices.

2. Large-Are Printing Techniques for Solution Processing

The solution synthesis method for large-area PSCs and PSMs can be mainly classified into following distinct categories: spray coating, gravure printing, screen printing, slot die coating, and blade coating.

2.1. Blade Coating

Blade coating, as an approach for fabricating perovskite thin-film solar devices, offers distinct advantages concerning cost-effectiveness, deposition of ultra-thin film, and simplicity compared to alternative methods. By employing a blade to uniformly disseminate the precursor solution, this printing approach facilitates meticulous control over various parameters throughout the manufacturing cycle (Figure 1a). It is particularly well-suited for roll-to-roll manufacturing processes, where continuous fabrication is desired. Additionally, blade coating allows for seamless integration with other deposition techniques, rendering it a versatile choice for thin-film device fabrication. The method minimizes material waste, conferring reasonable governance over thickness and temperature, and can be proficiently implemented under ambient conditions. These features engender its widespread applications and its pivotal role in fostering the developments of perovskite-based solar innovations [18,19].

2.2. Slot Die Coating

Slot die coating method has emerged as a highly promising (R2R) technique for high-volume manufacturing of perovskite-based solar devices. It offers several advantageous features, including reduced material wastage, precise adjustment of film thickness, and the capability for extensive area deposition. In the conventional slot die coating procedure, the precursor mixture is coated onto the moving web, filling the gap between the slot die head and substrate, as illustrated in Figure 1b. Upon solvent evaporation from wet film by drying and further solidification, a pinhole-free and uniform film can be obtained. A pre-metered slot die coating allows for meticulous thickness regulation ranging from 10 to several hundred micrometers by modulating the substrate speed, the flow rate of the precursor mixture, and the size of slot die head for coating area. Originally utilized to produce photographic films, optical films, and magnetic tape, this process has now been adapted to produce perovskite thin-film devices [20–22].

2.3. Screen Printing

Screen printing is an exceedingly all-around printing technique employed for the creation of thin films by transfer of solutions onto substrates through the utilization of a screen. Since its advent in the early 20th century, this method has facilitated the deposition of thick wet films, characterized by high viscosity and low volatility solutions. The screen-printing process entails deliberate movement of a squeegee in conjunction with the screen, thereby compelling the precursor mixture to uniformly dispersed across the base, as exemplified in Figure 1c. Notably, screen printing can find applicability in scenarios necessitating the coverage of expansive areas spanning several square meters of substrates [23,24].

2.4. Gravure Printing

Gravure printing represents an additional R2R tactic employed for the large-scale fabrication of uniformly coated and defect-free PSCs on pliable substrates. This method offers an efficient means of achieving cost-effective and high-speed assembly of PSCs with desired patterns. Gravure printing implements an engraved roller, which is immersed in an ink reservoir and features recessed regions that define the active ink transfer area. Once the recesses are repleted with ink, the roller begins to rotate, while a blade is engaged to remove surfeit ink from inactive regions. As illustrated in Figure 1d, the ink is displaced to the underlying material through the pressure put forth by an impression roller [25].

2.5. Spray Coating

Spray coating is a widely implemented deposition approach utilized for the generation of some thin-film devices. This method entails precise dispensation of printing ink onto a substrate via a nozzle, resulting in the generation of fine aerosol droplets (Figure 1e). Notably, this technique boasts advantages, namely, optimal material utilization and rapid deposition. The tiny-sized ink droplets are propelled towards the substrate by means of application of the gas jet. The process of heating the substrate during coating is typically employed to improve the contact with underlying film, thereby facilitating the attainment of uniform and flaw-free thin films [26].

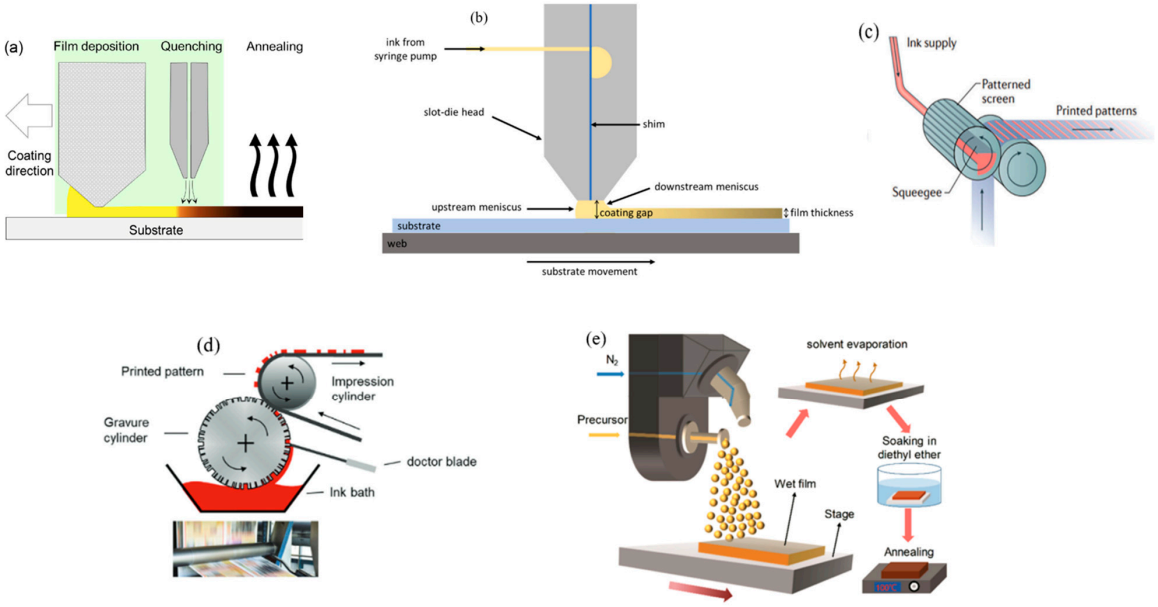

Figure 1. (**a**) Experimental arrangement and placement using the blade coating method [27], (**b**) Schematic of slot-die coating procedure [28], (**c**) Illustration of R2R screen printing [29], (**d**) Schematic of gravure printing on elastic substrate [30], (**e**) Schematic of spray coating process [31].

3. High-Efficiency Perovskite Solar Cells by Printing

Several noteworthy studies have shed light on the fabrication of high-performance PSCs by printing, offering significant insights into the successful implementation of blade coating, slot die coating, and screen-printing methods. These studies delve into various aspects, such as optimizing ink formulation, fine-tuning process parameters, and exploring post-treatment techniques, all of which contribute to achieving high-quality perovskite films and improved PSC performance. In the subsequent sections, notable studies are classified based on the coating method employed and subsequently elucidated in comprehensive detail.

3.1. Notable PSCs Based on Blade Coating

Incorporating a small amount of additives into perovskite precursor solution is an effective way to improve the performance of PSCs. The additives can help control crystallization, optimize film morphology, improve charge carrier transport, and passivate surface and grain boundary defects, thereby reducing non-radiative recombination. Jia et al. [32] introduced octane-1,8-diamine dihydroiodide (ODADI), a long carbon chain molecule, into wide bandgap (WBG) perovskite solution and utilized blade coating for fabrication of WBG PSCs. The ODADI doping suppressed intermediate phases, mitigated defects and facilitated crystallization in the perovskite films. Thus, the single junction inverted perovskite-based solar devices obtained PCEs of 19.63% (for an active area of 1.02 cm^2) and 22.06% (for an active area of 0.07 cm^2).

Zhang et al. [33] reported that incorporation of a small quantity of Cd in the form of CdI_2 in perovskite solution enhances the stability, inhibits non-radiative recombination, improves surface morphology, and better aligns band energies for $FAPbI_3$ perovskite-based solar devices. The Cd-doped $FAPbI_3$ was blade coated in air and corresponding PSCs show efficiencies of 22.7% for a 0.049 cm^2 area. The doping of Cd reduces defects, elevates charge carrier lifetimes, promotes charge harvesting, and leads to increased photovoltage. These findings highlight the potential of cadmium as an additive for improving the efficiency and stability of $FAPbI_3$-based photovoltaic cells.

Leveraging with a bifunctional additive in perovskite, p-aminobenzoic acid (PABA), Zhu et al. [34] have demonstrated an innovative scheme to synergistically mitigate defects and retard ion migration within inverted PSCs fabricated via scalable blade-coating technique. Comprehensive characterization has substantiated PABA's multifaceted benefits, including the effective inhibition of ion migration and diminishment of bulk defects within the perovskite film. Accordingly, the PABA-engine PSCs have shown performances up to 22.23% and 23.32% for device areas of 1 cm^2 and 0.1 cm^2, respectively, while PABA incorporated PSCs also exhibit remarkable operational stability, retaining approximately 94% of their performance after 1000 h of rigorous testing under one-sun radiation and at temperature of 75 °C.

Shi et al. [35] present a novel approach to address the limitations of organic semiconductors (e.g., PCBM and IDIC) for surface passivation in PSCs. Conventionally, these surface passivants have weak solubility in organic polar solvents and compatibility problems, which restricts their ability to penetrate and passivate the interior of perovskite films. To overcome this, the researchers account the easy synthesis of organic nanoparticles (NPs) that can disperse in perovskite printing solution. Organic NPs in the precursor solutions control the crystallization process and elevate film quality and conductivity, reaching holistic bulk film passivation. Consequently, the team successfully demonstrated PSCs with indene-C_{60} biadduct (ICBA) NPs and achieved an impressive performance of 25.1%. This work presents an effective process for comprehensive passivation by altering typical passivants into perovskite-fitting NPs, paving the way for the development of streamlined manufacturing of perovskite solar cells and modules.

Du et al. [36] present a compelling strategy to address the critical challenge of controlling defect formation and the nucleation-growth kinetics in ambient-printed $FAPbI_3$ perovskite films. Through a judicious combination of an additive, namely potassium

(3,5-difluorophenyl)trifluoroborate (PPTFB), and a cosolvent, 2-methyltetrahydrofuran (2MeTHF), the researchers effectively reduce the coordination between the perovskite and the solvent, as illustrated in Figure 2 and elucidated through comprehensive in-situ analyses. The study reveals that when the solvent has robust interplays with the perovskite, like commonly used DMF/DMSO solvents, the sol-gel states don't competently change into the desired α-$FAPbI_3$ phase, leading a diminished nucleation ratio and constrained crystal development directions, which ultimately prevents the fabrication of void-free perovskite layers. Oppositely, less strong solvent-perovskite interaction promotes the unmediated solidification, exhibiting more well-rounded nucleation and growth dynamics and mitigating the generation of microstrains and defects. This elegant approach with combination of 2MeTHF cosolvent and an PPTFB additive leads to remarkable improvements in the structural and optoelectronic properties of the $FAPbI_3$ films, including fewer defects, more closely packed grains, and smoother surface texture, diminished lattice deformation. The $FAPbI_3$ perovskite-based solar devices utilizing this strategy demonstrate performance of close to 24%, with improved performance stability as a reliable output, further underscoring the significance of this innovative solution-processing approach.

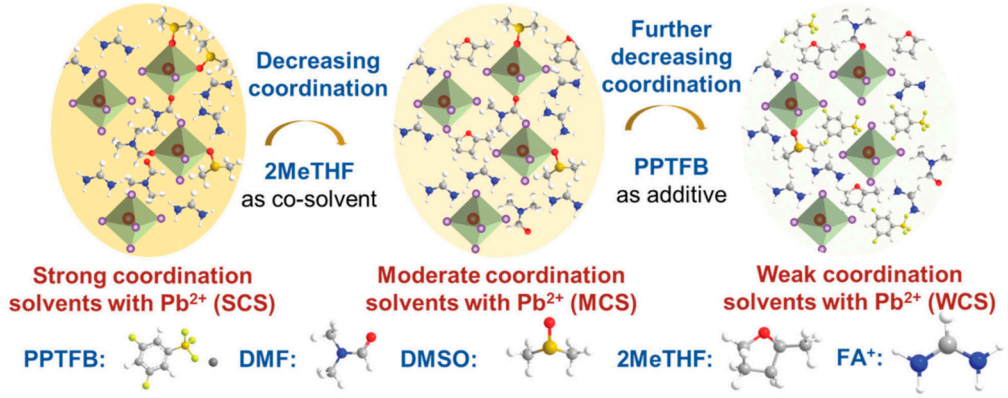

Figure 2. Schematic for combined cosolvent and additive strategy to reduce coordination regulation by replacing strong coordination solvent (SCS) with weak coordination solvents (WCS), [36].

Pu et al. [37] discovered that when wide-bandgap perovskite films were deposited using blade-coating, there exist uneven strains, including axial strain in the out-of-plane orientation and tensile strain in the in-plane direction, with the peak tensile strain occurring on the upper surface. These strains cause the deterioration of perovskite films by introducing more iodine vacancy defects. However, by performing mixed-cation post-treatments with 1,3-propanediammonium iodide (PDADI) and formamidinium iodide (FAI), they were able to relieve the strain and achieve uniformly crystallized perovskite films. Implementing this strain mitigation strategy, they produced high-quality methylamine-free WBG film by bade coating and accomplished PSCs with a remarkable performance of 19.45% for limited-area cells and a record PCE of 18.21% for 1 cm^2-area cells (see Figure 3). Notably, the PSCs with tension reduction kept approximately 109% of their primary efficiency after 400 h of operation, while the control structures declined to 91%. Moreover, the 4-terminal all-perovskite tandem solar cells acquired an optimized working performance of 27.64%. This strain release strategy with mixed PDADI/FAI post-treatment represents a viable pathway to boost PSC stability and performance by decreasing residual strains in perovskite thin films.

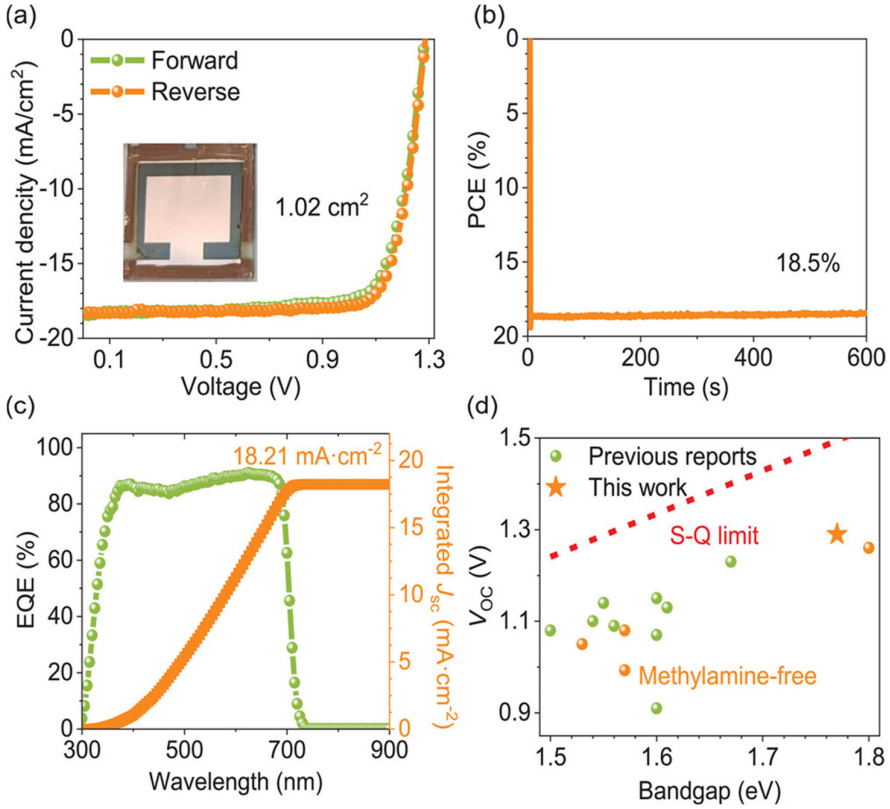

Figure 3. (**a**) J-V characteristics, (**b**) stabilized PCE over time, (**c**) EQE plot for blade coated PSCs with device area over 1 cm^2, (**d**) champion Voc for WBG-based PSCs [37].

The productivity of blade-coated tandem solar cells has been significantly enhanced through the implementation of additive scheme, as demonstrated by Subbiah et al. [38]. The incorporation of F6TCNNQ as a molecular impurity in the feedstock ink allows for the formation of micrometer-thick perovskite films that are conducive to textured silicon cells. Also, traditional organic hole transport layer of PTAA was substituted with a blended-type of self-assembled monolayer (SAM)-based hole selective layer merging Br-2PACz and MeO-2PACz molecules. Thus, the energy level mismatch between the perovskite absorber layer and the hole transporting layer is minimized, leading to improved device performance. In this work, the researchers synergistically combined these two strategies to elevate the efficiency of tandem cells. The utilization of F6TCNNQ as a molecular p-type impurity integrated in the feedstock ink improved the morphology and crystallinity of the blade-coated wide bandgap perovskite. As indicated in Figure 4, the resultant blade-coated perovskite/silicon tandem cells demonstrated a remarkable PCE of 29.7%, which presently stands as the highest reported efficiency for linear printing techniques. Moreover, the devices incorporating MeO:Br-2PACz showcased enhanced durability under maximum power point testing as compared to those utilizing only 2PACz. The 2PACz-based devices experienced a sharp decline in performance, while the MeO:Br-2PACz-based PSCs remained stable for longer time periods under 1 sun radiation.

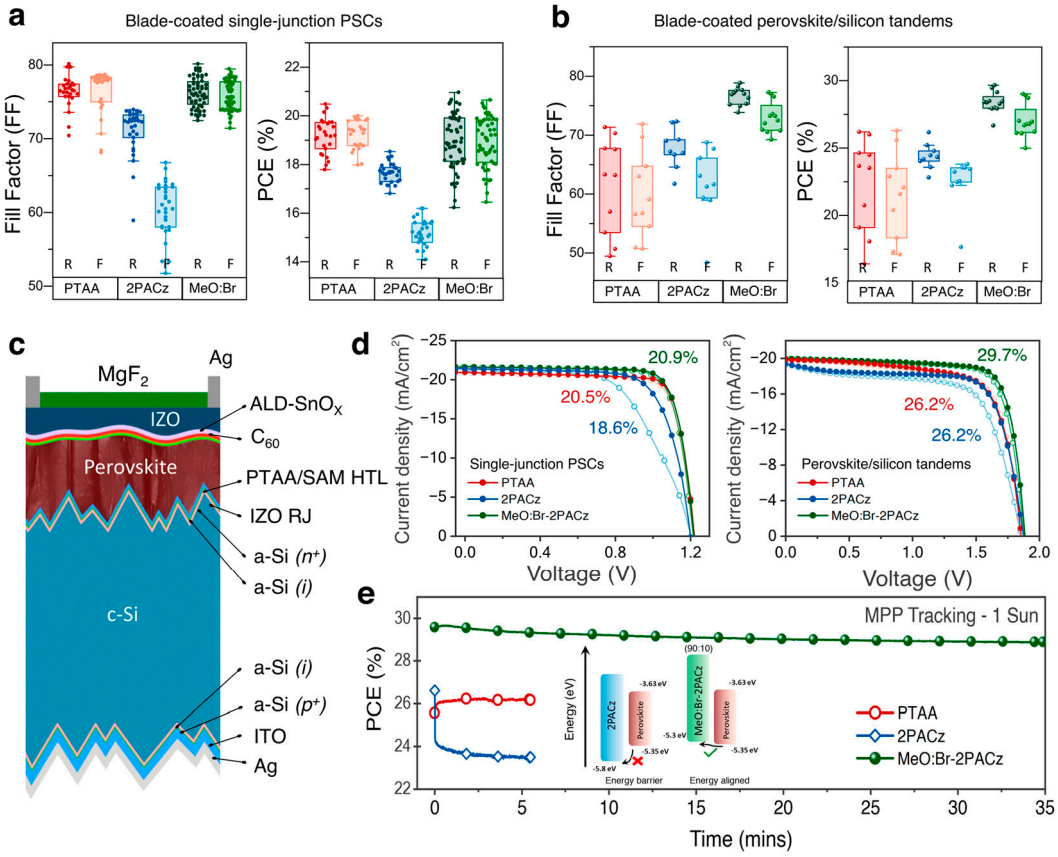

Figure 4. (**a**) Fill factor (FF) and PCE statistical distribution for blade-coated single-junction PSCs using different bottom contacts: PTAA, (MeO:Br)-2PACz, and 2PACz, (**b**) Statistical distribution of PCE and FF for blade-coating tandems with F6TCNNQ incorporation and different hole transport layer (HTL) (PTAA, (MeO:Br)-2PACz and 2PACz), (**c**) unit architecture of F6TCNNQ-doped tandems with different HTL configurations, (**d**) J-V curves of single junction (hollow circles) and tandem devices with different HTLs, (**e**) MPPT stability testing of blade-coated tandem solar cells [38].

In addition to additive strategy, solvent engineering, interfacial engineering, and surface passivation are also widely used to improve performance of printed PSCs. Liang et al. [39] proposed a controllable cosolvent method for fabricating PSCs using a blade coating technique at room temperature in the presence of both the 2-methoxyethanol (2-Me) and methylammonium acetate (MAAc) solvents. This cosolvent scheme allows for better control over the perovskite crystallization, resulting in improved film uniformity and reproducibility through blade coating. The use of a benzohydrazide as passivation layer further enhances cell performance and stability. The champion PSC reached a superior fill factor of 82.8%, and PCE of 20.11% in inverted $MAPbI_3$-based devices (0.052 cm^2). The study also demonstrated high device stability and reproducibility, with 95% of the initial PCE maintained for approximately 800 h in ambient conditions.

Mariotti et al. [40] focused on boosting the performance of two-terminal monolithic perovskite-silicon tandem solar cells (see Figure 5). By surface treatment of a triple-halide perovskite with piperazinium iodide (PI) molecules, the researchers achieved enhanced band energy alignment, reduced recombination losses, and improved charge extraction as compared to the commonly used LiF interlayer. The tandem solar cells demonstrated open-circuit voltages and achieved efficiencies of up to 2 V and 32.5%, respectively. The tandem cells with PI interfacial treatment demonstrated improved operational reliability, securing 75.7% of the initial efficiency after 478 h and 80% after 347 h of continuous MPPT tracking operation.

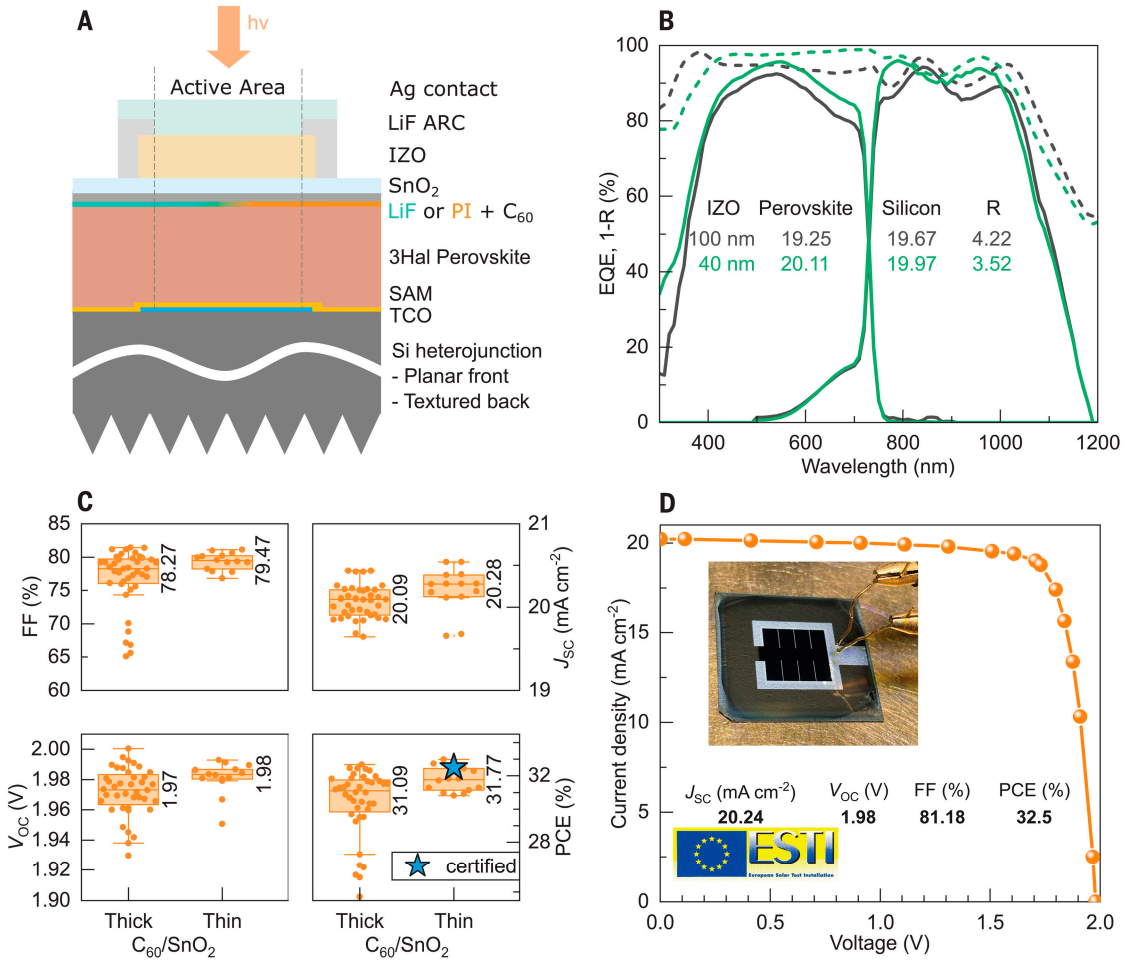

Figure 5. (**A**) Schematic view of the tandem-structured device, (**B**) Measured reflection (1-R) and EQE of mentioned tandem solar cells, (**C**) Photovoltaic parameters of tandem solar cells with variation in thickness, (**D**) Quasi steady-state J-V characteristics [40].

The PSC's interfaces are paramount in determining their stability and efficiency. Chen et al. [41] observed that partial substitution of DMSO with solid-state carbohydrazide mitigates the gaps at the perovskite bottom surface, enabling blade-coated p-i-n PSCs to attain a maximum efficiency of 23.6% without efficiency erosion after 550 h of operational reliability testing at 60 °C. Furthermore, they demonstrated min-modules with PCEs of 19.2% and 19.3% for aperture areas of 50.0 and 18.1 cm^2, respectively. This study underscores the paramount importance of optimizing the perovskite-substrate interface to unlatch the complete potential of PSCs and advance their commercial viability.

Wang et al. [42] developed an innovative polymeric electron transport material, namely PFBCP, by polymerizing BCP and C_{60}. PFBCP ETL requires only one-step deposition, contrary to commonly used C_{60} deposition followed by BCP coating, accomplishing not only efficient electron transport and hole blocking, but also minimizing interface recombination thereby enhancing performance stability. Consequently, their blade-coated PSCs employing PFBCP as ETL attain a PCE surpassing 22% and secure 91% of their initial PCE after 1200 h of light illumination.

Yang et al. [43] demonstrated the production of large-area perovskite-silicon tandem cells utilizing a blading coating step. A lithium fluoride (LiF) layer was introduced between perovskite absorber and PTAA HTL (Figure 6) to reduce shunt leakage from non-uniformity coating of perovskite layer, attaining PCE of 25.1% for 24 cm^2 tandems. The use of different bottom cell surface morphologies (polished FZ, etched CZ, and textured CZ) showed comparable efficiencies, but process yields varied. The LiF interlayer improved yields in

etched CZ tandems. Overall, this research demonstrated high-efficiency tandems while addressing shunting challenges in the large-area fabrication with blade coating process.

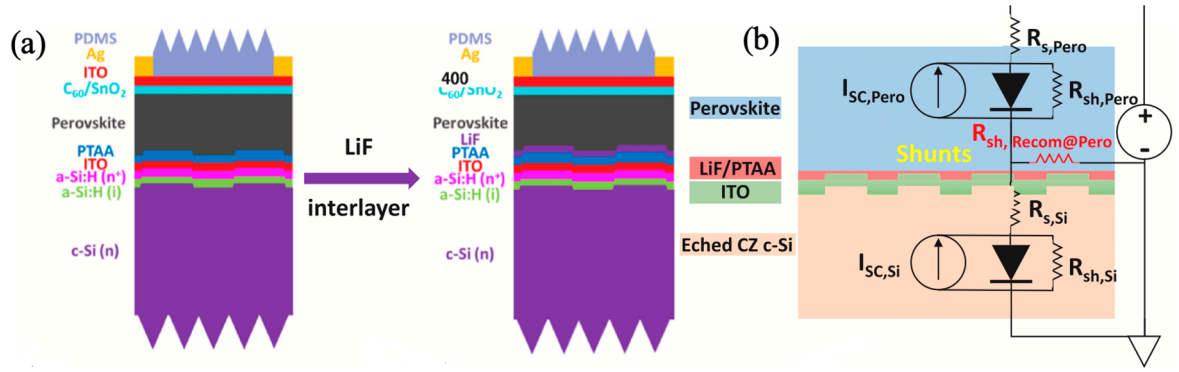

Figure 6. (**a**) Structure of perovskite-silicon tandem solar cells without and with LiF layer, (**b**) Schematic of equivalent circuit of the tandem cell [43].

3.2. Notable PSCs Based on Slot Die Coating

Xu et al. [44] focused on composition engineering to develop a superior triple-halide perovskite material for fabrication of PSCs utilizing slot-die coating technique. The perovskite composition of 5 mol% $MAPbCl_3$ + $(Cs_{0.22}FA_{0.78})Pb(I_{0.85}Br_{0.15})_3$ was optimized for slot-die coating. By carefully controlling the annealing and drying conditions, they achieved high-quality films with improved photoluminescence and ample crystalline grains, reducing charge recombination losses. Figure 7 demonstrated high stability and PCE of up to 19.4%. Furthermore, by merging the perovskite layer with optimal bandgap of 1.68 eV with commercial silicon cells, a tandem PSC with a power conversion efficiency of 25.2% on a 1 cm^2 area was attained. These developments highlight the potential of slot-die coating for scalable fabrication of efficient perovskite-silicon tandem solar cells.

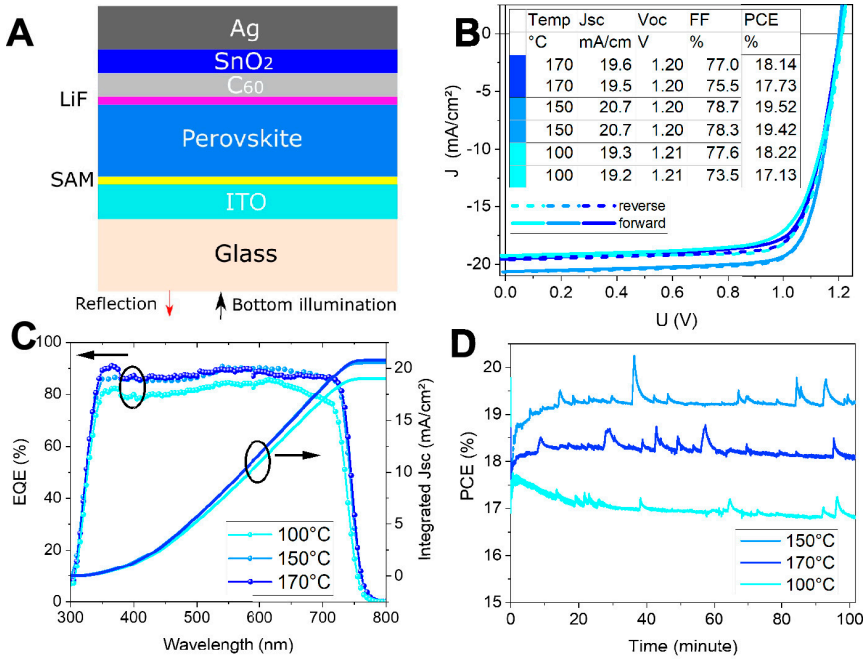

Figure 7. (**A**) Structure of the single-junction perovskite sub-cell for integration with commercial silicon cells, (**B**) J-V plots of champion PSCs optimized at varying annealing temperatures, (**C**) External quantum efficiency measurement and integrated short-circuit current, Jsc, (**D**) MPPT stability test of the fabricated best solar cells at 25 °C [44].

Additive engineering approach was employed to attain high-quality perovskite thin films by slot-die coating [45]. They employed potassium thiocyanate (KSCN) as an additive to augment the quality of $MAPbI_3$ perovskite absorber. The modified films exhibited a mean grain size of approximately 11 µm, showcasing charge-carrier characteristics akin to those of single-crystal perovskites. The PSCs with little hysteresis demonstrated a mean PCE of 20.14% and a highest PCE of 21.38% with device effective area of 0.089 cm^2 (see Figure 8). Importantly, the fabricated PSCs with slot-die coating showed a narrow PCE variation, reinforcing the potential of the slot-die coating technique for the large-scale manufacturing of high-efficiency PSCs. The study also employed a methylamine (MA)/acetonitrile (CAN) complex as low boiling solvent, as opposed to the traditional dimethyl formamide (DMF)/dimethyl sulfoxide (DMSO) mixture, to avoid high-temperature annealing and safeguard the underlying PTAA hole transport layer, which was blade coated.

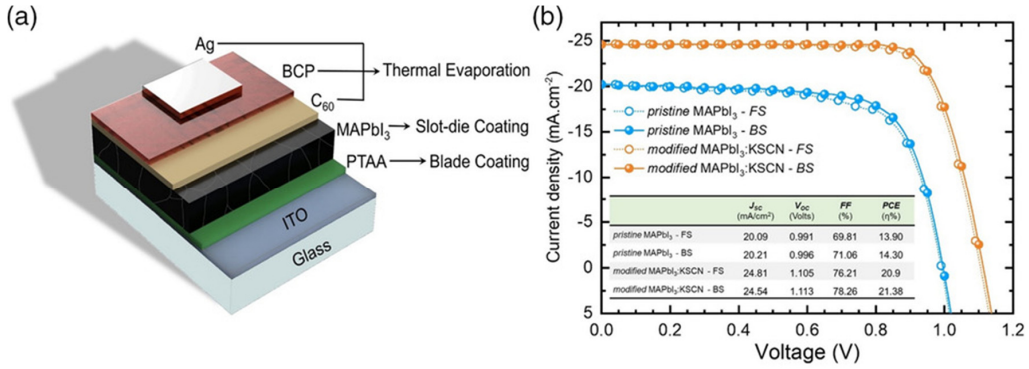

Figure 8. (**a**) Device structure and deposition approach for each layer, (**b**) J-V plots of the best PSCs based on pristine and KSCN incorporated $MAPbI_3$ films [45].

Li et al. [46] boosted the efficiency and scalability of PSCs by implementing solvent engineering and slot-die coating. By incorporating dimethyl sulfoxide (DMSO) as additive to the perovskite ink formulation, in which 2-methoxy-ethanol (2-ME) serves as low boiling point green solvent, the solar cells achieved a maximum PCE of 20.8% (active area is 0.16 cm^{-2}), as indicated in Figure 9, The optimal quantity of DMSO was approximately 12 mol%, which improved the coating properties and suppressed the formation of undesirable intermediate phases. However, excessive DMSO content led to the precipitation of a detrimental solvate phase. The study emphasizes the necessity of precise ink composition and processing conditions for reproducible large-scale production of PSCs.

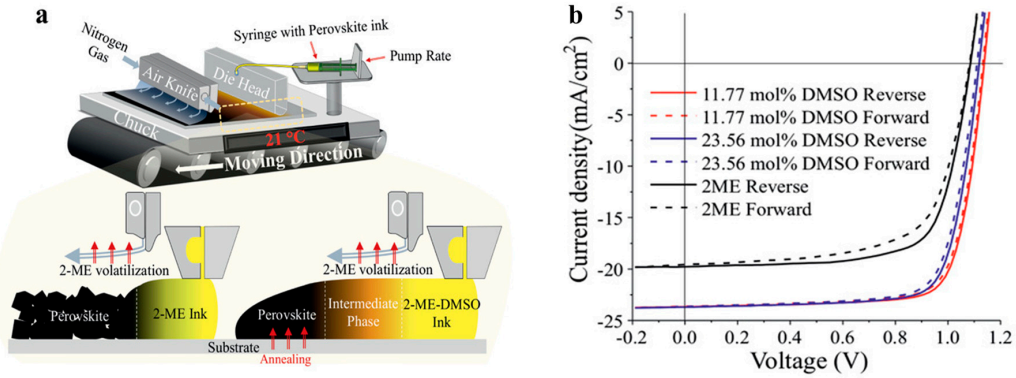

Figure 9. (**a**) Illustration of slot die coating setup, (**b**) J-V plots at various DMSO additive solvent concentrations [46].

Abate et al. [47] aimed to improve the efficiency and reliability of large-area PSCs with surface passivation. They fabricated consistent perovskite films using a slot die coater on a c-TiO_2 layer. The films were modified with a novel artificial peptide, sulfonyl-γ-

AApeptide (F-GLU-S), which interacted strongly with the perovskite absorber to repair the uncoordinated Pb^{2+} ions and halide vacancies, thereby, significantly diminishing non-radiative recombination. The passivated devices achieved maximum efficiency of 21.44% with 10 × 10 cm^2 active area and retained approximately 92% of their initial performance after 720 h in air.

Rana et al. [48] stated the advancement of a more balanced surface passivation method for perovskite absorber. The passivated perovskite layers demonstrated several beneficial characteristics, including higher photoluminescence (PL) intensity, apparent larger grain size, better spatial PL uniformity, and reduced recombination rates as evidenced by longer PL lifetimes. The PSCs with optimized passivation layer depicted a high performance of 20.3%, a huge progress over the 18.7% PCE obtained for the control device. The researchers applied an isopropanol (IPA)/BAI solution onto the pre-deposited perovskite film, which was heated to 40 °C, and then immediately annealed at 100 °C for 1 min, a process designed to rapidly evaporate the IPA and leave only a minimal amount of residue within the perovskite films. The study was initially conducted on limited-area devices (effective area of 0.0453 cm^2) before being expanded to larger area samples, with the 1 mg/mL Benzylammonium idodide (BAI) concentration found to yield the best device efficiency, and the passivated device exhibiting small hysteresis in its current properties.

In the pursuit of commercializing PSCs, the advancement of industrially compatible printing techniques for stable, efficient, and cost-effective charge transporting layers is of paramount importance. Zimmermann et al. [49] presented the first-ever demonstration of copper thiocyanate (CuSCN) as a reliable and low-cost hole-transport layer utilizing the slot-die coating technique. By employing an asymmetric cosolvent, methyl ethyl sulfide, the solubility of CuSCN was enhanced, making a markable improvement over the diethyl sulfide-based mixtures. This CuSCN inks enable slot die coating of CuSCN HTL on substrate as large as 10 × 5 cm^2, with a well-controlled thickness. Utilizing advanced photoluminescence characterization, the study investigates the influence of solvents on charge carrier recombination and losses and the thickness uniformity of the slot die coated CuSCN thin films. Ultimately, the integration of the CuSCN HTL into the PSC, along with slot die coated perovskite absorber, has yielded impressive results, demonstrating power conversion efficiencies of 14.7% for 9 cm^2 minimodules and 19.1% for small laboratory cells. Remarkably, the semitransparent minimodules have retained 80% of their initial performance even after 500 h of one-sun radiation, underscoring the stability of slot die coated PSCs and minimodules.

3.3. Notable PSCs Based on Screen Printing

The utilization of carbon counter electrode in mesoscopic perovskite solar devices has gained considerable attention owing to their remarkable long-term stability and suitable for screen-printing under ambient conditions. Sheng et al. [50] developed a carbonaceous material based on phenol-formaldehyde resin for use as the counter electrode in printable mesoscopic perovskite solar cells (p-MPSCs). The study showed that at optimized quantity of H_2O/EtOH ratio (3/4), the infiltration of the perovskite precursor ink into the electrodes was largely elevated due to the interaction between the chemical functional groups of the produced carbon substance and Pb^{2+}. Consequently, the open-circuit voltage (Voc) was enhanced from 0.97 V to 1.03 V, leading the highest efficiency of 17.64% for the new carbon-based p-MPSCs. This work presents an effective strategy to develop carbon-based counter electrodes for highly stable and high-performance p-MPSCs.

Chen et al. [51] developed a stable and adjustable perovskite solution made from an ionic liquid solvent for screen-printing of MPSCs. The screen-printing technique allowed for control over the area and thickness of the perovskite films on different bases. They achieved high printing rates of 20 cm s^{-1} and close to 100% ink utilization. The best efficiencies obtained were 18.12% for a 1 cm^2 effective area and 20.52% for a 0.05 cm^2 active area, surpassing the reference performance based on spin-coated films. Fully screen-printed PSCs with device structure of FTO/c-TiO_2 (60 nm)/m-TiO_2 (1200 nm)/m-ZrO_2

(200 nm)/perovskite/carbon (50 µm) were also demonstrated, in which each layer was screen printed in air. The corresponding PCEs are 14.98% with device are of 0.05-cm^2, and 11.80% for mini-module with area of 16.37 cm^2. The PSCs with all screens printed stacking layers showed good stability, remaining over 95% of initial efficiency over 300 h under operational maximum power point stability testing. This study indicated that screen printing method allowed for the fabrication of patterned films and could be applied to each functional layer with various thickness. The same group further explored the utilization of a co-solvent strategy involving an ionic liquid mixture comprising methylamine acetate (MAAc) and methylamine propionate (MAPa) for the fabrication of fully screen-printed PSCs [52]. The target of this approach is to increase the crystallization as well as the stability of screen-printed perovskite films. The introduction of MAPa enables the controlled escape of MAAc ionic liquid, resulting in enhanced crystalline quality and increased perovskite crystal's filling degree within the m-TiO_2/m-ZrO_2 mesoporous network. MAPa also facilitates the vertical growth of perovskite lattices, refines the energy level alignment at the perovskite/carbon electrode interface, thereby enhancing charge transport and harvesting. At the optimized co-solvent ratio of 75% MAAc and 25% MAPa, fully screen-printed PSCs yield a champion efficiency of approximately 17%. With the similar device structure to report [52], Zhu et al. [53] presented another solvent engineering approach to produce MPSCs. Three mesoporous layers were sequentially deposited onto c-TiO_2 using screen printing, then sintered for 35 min at temperatures of 500 °C, 450 °C, and 400 °C. The layers included a mesoporous-TiO_2 (m-TiO_2) layer about 500 nm thick, a mesoporous-ZrO_2 (m-ZrO_2) spacer layer approximately 2 µm thick, and a carbon layer roughly 10 µm thick. A mixed solvent comprising N-methyl-2-pyrrolidone (NMP) and 2-methoxyethanol (2-ME), along with ammonium chloride (NH_4Cl) as a crystallization agent, was introduced into perovskite precursors, as shown in Figure 10. The optimized coordination environment created by the NMP/2-ME mixed solvent enabled uniform perovskite crystallization at room temperature without thermal annealing step. The addition of NH_4Cl effectively regulated the perovskite crystallization, resulting in well-defined perovskite films. The MPSCs fabricated through this solvent engineering accomplished a champion performance of 17.34%. Also, high-quality films from screen printing result in good long-term air durability, retaining relatively 98% of the initial efficiency after 203 days under ambient indoor conditions. This research provides valuable insights into simplifying the fabrication process of MPSCs while achieving significant improvements in efficiency and stability.

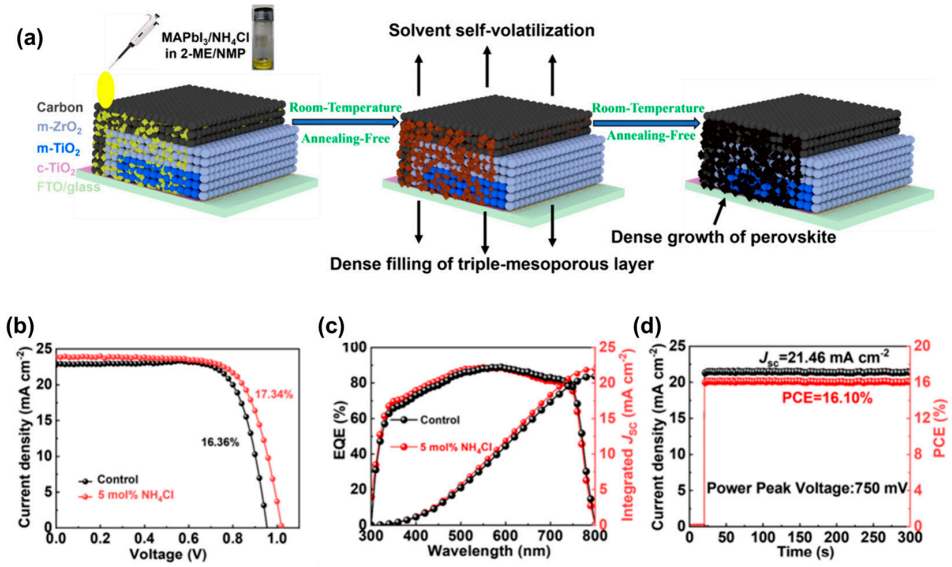

Figure 10. (**a**) Schematic of perovskite crystallization with additive and cosolvent strategy, (**b**) J-V plots of fabricated PSCs, (**c**) EQE for both cases of with and without NH_4Cl, (**d**) MPPT stability testing of PSCs with optimized NH_4Cl addition [53].

He et al. [54] developed an approach for acquiring high-efficiency printable MPSCs by considering the multidentate molecule 6-chloropurine (6-CP) as passivation agent. Through the study of density functional theory (DFT) calculations and spectroscopic characterizations, they demonstrated the competition mechanism of bidentate coordination among the chlorine atom of 6-CP and neighboring nitrogen atoms. This bidentate passivation strategy improved charge transfer, hole selectivity, and reduced nonradiative recombination, leading to enhanced efficiency and reliability under high humidity situations. They also discovered that the bidentate coordination primarily occurred between under-coordinated Pb^{2+} ions and adjacent nitrogen N_2 in the imidazole ring. The fully printable PSCs were fabricated using a combination of spray pyrolysis for TiO_2-dense layer (c-TiO_2) and screen printing for mesoporous TiO_2 (m-TiO_2), mesoporous ZrO_2 (m-ZrO_2), and carbon contact, achieving champion PCE of 17.63% over an active area of approximately 0.64 cm^2. The results highlight the potential of selective bidentate passivation for printable PSCs and provide insights for future molecular passivation design.

The employment of potassium hexafluorophosphate (KPF_6) in perovskite to produce fully screen-printed MPSCs has been demonstrated as an efficacious passivation additive to surmount the lingering issues of defects and filling mesopore layers that hinder the MPSC performance [55]. Rigorous investigations on the material properties and the corresponding MPSC efficiencies revealed that the incorporation of KPF_6 substantially enhances crystallinity, mitigates defect states, and facilitates perovskite infiltration within the mesoporous framework, collectively suppressing non-radiative recombination losses and leading to concomitant enhancement in efficiency and operational stability. Specifically, the champion MPSC devices incorporating the KPF_6 additive yielded an optimized efficiency of 15.39%, representing a remarkable ~10% improvement over the control systems (14.16%). Moreover, the unencapsulated MPSCs kept 95% of their initial efficiency after 50 storage days at ambient environments, whereas the control MPSCs without KPF_6 only maintained 80% of their primary efficiency.

Overall, in the context of producing high-efficiency PSCs using high-speed printing techniques, it is crucial to understand the pros and cons for each specific printing method implemented in manufacturing of PSCs. Herein, Table 1 presents a comprehensive overview of three mentioned coating techniques—screen printing, slot-die coating, and blade coating—used in the fabrication of PSCs. Each approach is examined in terms of its advantages, underlying scientific principles, and associated issues. This comparative evaluation aims to elucidate the weaknesses and strengths of different printing techniques, providing perspectives in their applicability in large-volume manufacturing and operating efficiency optimization of PSCs. By fully understanding and considering these aspects, scientist and manufacturers can make decisions to choose the most appropriate coating scheme to accomplish their aimed efficiency and reliability of PSCs, thereby aiding to the developments of solar technology innovations by printing.

Table 1. Comparative evaluation of coating techniques commonly used for PSC fabrication.

Techniques	Crucial Scientific Aspects	Advantages	Challenges
Blade coating	Utilize a blade to spread solution across a substrate and form a layer after drying, relying on gravity and surface tension	High throughput and operating efficiency. Capable of making thinner, uniform layers	Limited to low-viscosity solutions. Risk and shortcomings include streaking, and requires precise control of coating speed
Slot die coating	Uses a narrow slot to control the flow of ink, creating uniform wet film	High precise layer thickness and uniformity. Scalable for extensive surfaces. Appropriate for continuous production	Higher primary component costs. Needs precise control and coordination of ink viscosity, web speed, and flow rates to accomplish target thickness

Table 1. *Cont.*

Techniques	Crucial Scientific Aspects	Advantages	Challenges
Screen printing	Involves forcing solution within a mesh screen, generating patterns introduced by the stencil	Cost-effective for limited-scale production. Versatile for various bases and can handle low-viscosity solution to create thick films	Lower resolution than other schemes. Potential for inconsistent film thickness and slower speeds for extensive areas

4. Large-Scale Coating from Cells to Modules and Fully Printed PSCs and PSMs

When the dimensions of the photovoltaic cells are increased, there is a resultant reduction in overall efficiency [55–57]. This efficiency degradation is not unique to perovskite technology and has also been observed in other established thin-film technologies [58,59]. However, the more pronounced efficiency drop observed in perovskite modules can be primarily ascribed to issues such as film quality, the presence of defects, contamination, and non-uniformity across large area [60,61]. To establish commercial viability, it is imperative to demonstrate the scalability of this perovskite-based photovoltaic technology without compromising its PCE. Encouragingly, large-area modules (810 cm^2) and mini-modules (26.02 cm^2) have been certified with PCE values of 18.6% and 22.4% respectively, showcasing the successful upscaling of the perovskite solar technology. Also, PSCs have been effectively integrated with silicon photovoltaics in tandem configurations, demonstrating an impressive PCE of 33.9% on small-area devices [62]. These achievements are crucial for substantiating the potential of perovskite-based photovoltaics and paving the way for their practical application in the market.

When printing technologies come to scaling up PSCs to PSMs, Sheet-to-Sheet (S2S) and Roll-to-Roll (R2R) processes are commonly employed. These manufacturing methods involve depositing and processing materials in either a roll or sheet format, offering numerous advantages for large-area coating in mass production of PSMs. In the R2R printing, the substrate is continuously fed into a processing system where coating and other fabrication steps occur in a seamless flow. This method best fits continuous printing on flexible substrates and enables high throughput and efficient use of materials, making it ideal for large-scale production. Coating techniques, such as aforementioned blade coating, slot die coating, and screen printing can be adapted for R2R processing. On the other hand, the S2S approach involves processing individual sheets or panels. Each sheet is coated and processed separately before being assembled into a module. This approach provides greater flexibility in terms of process control and optimization since each sheet can be treated individually. It is commonly utilized for smaller-scale production or when specific customization is necessary. Both R2R and S2S approaches necessitate careful consideration of coating techniques to ensure uniformity, quality, and scalability. By effectively implementing R2R or S2S processes and selecting the most suitable coating techniques, researchers and manufacturers can achieve high-performance PSCs and PSMs on a larger scale. High-quality printing process not only boosts the stability, efficiency, and reliability of solar modules but also enables cost-effective mass production, driving the commercial viability of perovskite-based photovoltaics.

In this section, some fully printed PSCs and PSMs are examined to demonstrate progress in fabrication of perovskite-based solar cells and modules by high-speed printing. Weerasinghe et al. [63] presented a groundbreaking achievement of creating PSCs and PSMs utilizing R2R printing of all stacking layers (including contact) in industrial setting Traditional metal electrodes were replaced with carbon electrodes, significantly reducing costs. The printed PSCs and PSMs have device structure of PET/Transparent Contact Electrode (TCE)/SnO_2 ETL $FA_{0.45}MA_{0.55}PbI_3$/n-hexyl trimethyl ammonium bromide (HTAB) passivation layer/P3HT HTL/Carbon/Ag, in which SnO_2 ETL was deposited using reverse gravure coating, the remaining layers up to carbon contact are deposited by slot-die coating, the optional Ag contacts are screen printed as shown in Figure 11. Through a

high-throughput experiment, researchers optimized the R2R fabrication process, resulting in individual limited-area cells with a maximum efficiency of 15.5% and extensive-area modules with serially interconnected cells accomplishing a PCE of 11.0% (active area of about 50 cm^2). The successful demonstration of R2R-printed PSCs and PSMs using high-speed printing of all stacking layers represents a significant advancement toward commercialization of perovskite-based photovoltaics. The estimated cost for large-scale production in Australia is approximately $0.7 USD per watt, with potential for further cost reductions.

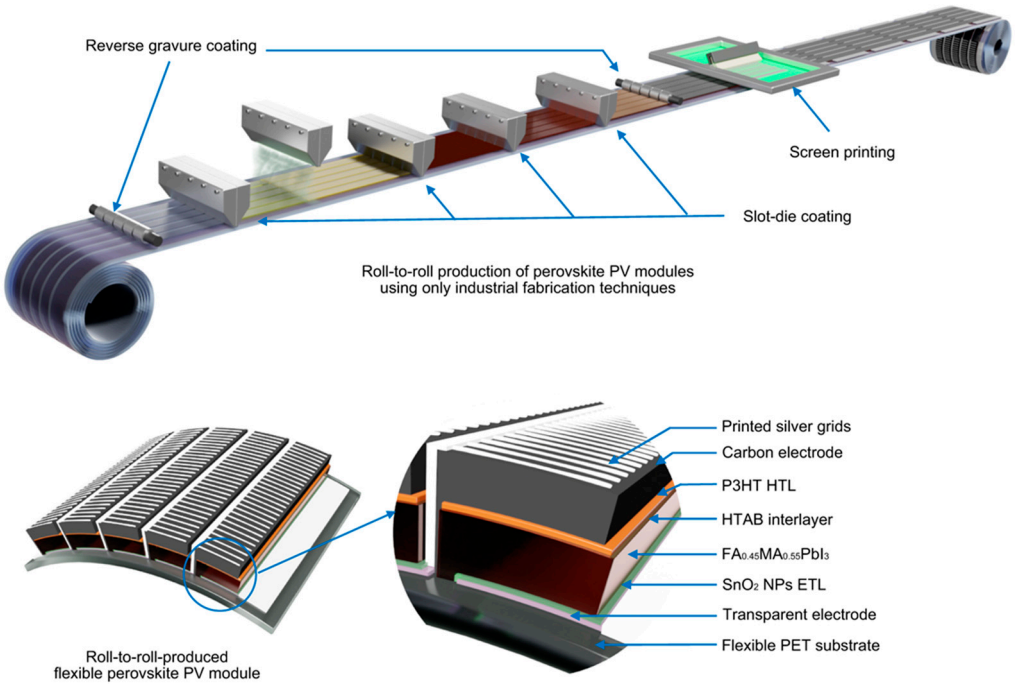

Figure 11. Illustration in printing procedure and resulting structure of fully R2R printed PSMs [63].

Vesce et al. [64] successfully fabricated perovskite sub-module over large area in ambient condition with combined meniscus coating techniques, including slot-die coating of perovskite absorbing layer and blade coating of surface passivant, phenethylammonium iodide (PEAI). They employed a passivation strategy on perovskite with PEAI and engineered the perovskite precursor mixture with acetonitrile (ACN) solvent for better film quality. The surface passivation and solvent engineering resulted in an optimized performance of 16.13% for PSMs over an aperture area of 201 cm^2, with minimal losses compared to smaller cells. Characterization techniques confirmed layer homogeneity, and the sub-module demonstrated stability for over 3000 h. Life cycle assessment highlighted its economic and environmental advantages, including efficiency, stability, sustainability, and cost-effectiveness in the reported PSMs.

4.1. Fully Blade Coated PSCs and PSMs

Carbon-based PSCs have shown promise for improved stability and low-cost production in ambient air. However, achieving high-efficiency carbon-based modules requires uniform deposition of void-free perovskite layer over extensive areas, which remains a significant challenge. Ren et al. [65] introduced a long chain gemini surfactant into the perovskite precursor solution to enhance film coverage and smoothness. The surfactant played a collaborative role in perovskite layer creation, modulation of solidification dynamics, and defect passivation. As a result, they achieved a certified performance of 15.46% for the modules, with a Jsc of 22.92 mA cm^{-2} and Voc of 1.13 V. Importantly, all functional layers were printed using a high-speed blade coating tool in ambient condition. This development represents an important step towards the industrialization of carbon-based perovskite solar

modules. Additionally, by incorporating long chain gemini surfactants, the team fabricated a fully printed carbon-based module with an effective area of 50 cm^2 and attained a PCE of 17.05%. This latest result proves that the gemini surfactants effectively reduced inhomogeneous solidification and improved the capillary behavior of the perovskite precursor solution during blade coating, resulting in best-quality perovskite films.

4.2. Fully Slot-Die Coated PSCs and PSMs

Producing large photovoltaic modules with online consistent R2R deposition of perovskite and transporting layers represents a big obstacle. Burkitt et al. [66] demonstrate R2R slot-coating of all stacking layers to fabricate p-i-n structured PSCs on a plastic substrate. The target PSCs have device architecture of PET/PEDOT:PSS HTL/Perovskite absorber/PCBM ETL/BCP interlayer/Silver (thermal evaporation), in which all solution processing layers are slot-die coated with constant coating speed of 1m per minute. Researchers employed a combination of singular perovskite ink and acetonitrile solvent set and devised a R2R slot-die coating procedure. They found that drying step is critical in achieving high performance PSCs. The resultant demonstrated stabilized performance of 12.2%, which is the highest PCE attained from PSCs fabricated by R2R-slot-coating of all stacking layers. This investigation underscores the viability of R2R printing for perovskite-based solar cells, proving the potential for fully inline R2R manufacturing of PSMs.

Teixeira et al. [67] focused on the optimization and development of low-cost and flexible PSCs with slot die coating of all stacking layers. The goal is to create a manufacturing process that is compatible with extensive-scale production while maintaining high performance and stability. The device architecture consists of four layers, including SnO_2 ETL, a mixed-halide 3D perovskite absorber $(FAPbI_3)_{0.85}(MAPbBr_3)_{0.15}$), a 2D perovskite capping/passivation layer (n-octylammonium iodide—OAI), and a carbon-based electrode. The whole device was fabricated by printing, in which SnO_2 ETL, 3D perovskite absorber, and 2D perovskite capping/passivation layer were slot die coated, and carbon electrode was blade coated. All these coating steps are fully compatible with large-scale manufacturing. The fabrication process involves carefully selecting solvent systems, determining coating windows for each material, and optimizing the manufacturing process. The resulting PSC demonstrated a highest PCE of 18.6% under 1 sun with an effective area of 0.64 cm^2. The 3D perovskite device showed good reliability, keeping 96% of its primary performance after 550 h of testing. However, the addition of a 2D layer negatively affected reliability because of accelerated ion diffusion among the 3D and 2D perovskite layers.

Li et al. [68] sought to establish a scalable printing paradigm for perovskite solar cells and modules utilizing slot-die coating for all stacking layers, which is fully compatible with large-scale ambient manufacturing. The researchers successfully deposited each stacking layer of p-i-n configured devices comprising a fluorine-doped tin oxide anode (15 ohm/sq), nickel oxide hole transport layer (40 nm), methylammonium lead triiodide perovskite absorber layer (300 nm), [6,6]-phenyl-C_{61}-butyric acid methyl ester electron transport layer (40 nm) through a slot-die coating methodology employing non-toxic solvent, including ethanol for the nickel oxide (0.1 M), dimethyl sulfoxide:2-methoxyethanol for the perovskite (29.20% by weight), and o-xylene:anisole for the $PC_{61}BM$ (15 mg/mL). With optimized solution concentration, layer thickness, and thermal annealing temperature and duration, slot-die printed PSMs with active area of 0.75 cm^2 yielded champion efficiency of 13.54%.

4.3. Fully Screen-Printed PSCs and PSMs

Fully printable MPSCs offer great promise as scalable, stable, and cost-effective photovoltaic devices, which normally consist of sequentially screen-printed layers of mesoporous TiO_2, ZrO_2, and carbon for perovskite infiltration, on the TiO_2 compact layer (C-TiO_2). The potential of screen-printing as an alternative to spray pyrolysis deposition for C-TiO_2 layer was investigated by Raptis et al. [69]. The MPSCs with screen-printed C-TiO_2 yielded similar PCE as compared to spray pyrolysis whenever the layer thickness is close to each

other. $TiCl_4$ treatment on C-TiO_2 is critical to accomplish a champion PCE of 13.11% for the cells with active area of 1 cm^2. These findings demonstrate the viability of screen-printing for fabrication of carbon-based MPSCs, offering potential for commercially competitive in manufacturing of highly efficient MPSCs with all stacking layer screen printed.

5. Assessments of High-Efficiency Perovskite Solar Modules

Producing large-area PSMs introduces a myriad of issues related to reliability, uniformity, and scalability of the perovskite film and other functional layers, which are crucial for accomplishing long-term performance, including both efficiency and stability. High-speed printing over large area normally causes inhomogeneities and flaws in the printed films, which serve as the non-radiative recombination centers that limit charge carrier transport and harvesting. Also, the sensitivity of perovskites to surrounding environments, such as UV radiation, moisture, and heat, can cause performance degradation, thereby negatively impacting the stability and lifespan of the created solar modules. Well addressing these problems is the key for the successful commercialization of large-area PSMs. In this section, a comprehensive evaluation of various high-performance perovskite solar modules (PSMs) is conducted, considering their heterogeneous dimensions, efficiencies, and fabrication methodologies. Three principal metrics about device area are conventionally utilized to assess the performance of PSMs: active area, aperture area, and total area efficiencies. Active area efficiency pertains to the energy-contributing segment of the module, while aperture area efficiency encompasses the internal interconnection regions. Total area efficiency assumes greater significance for practical applications in the field.

5.1. Notable PSMs Based on Blade Coating

Despite fast-paced advancements in perovskite-based photovoltaics, the degradation of perovskite film and the challenges in large-scale manufacturing under air have hindered the betterment of PSC outcomes. In this groundbreaking study, Yang et al. [70] unveiled an innovative ring-structured molecule, namely cyclen, for creation of top-notch perovskite films. For the first occasion, the researchers have secured a vital intermediate, cyclen-PbI_2-DMSO, which postpones the crystallization process, decreases non-radiative recombination, and promotes carrier lifetime. Through detailed experimental characterization and DFT calculations, the team has demonstrated that the cyclen interacts effectively with Pb^{2+} ions, thereby modulating the crystallization and reducing defect density. Subsequently, the limited-area device fabricated using this addition approach achieved a remarkable performance of up to 24.71% and was able to keep 90% of its initial PCE. Moreover, large-area (36 cm^2) PSMs yielded PCE of 20.08%, where cyclen-regulated perovskite was blade-coated in ambient settings.

Defects induced by interstitial iodides are a main restriction in perovskite solar devices affecting their efficiency and stability. However, the introduction of a little amount of ($Zn(OOSCF_3)_2$ in the perovskite mixture can effectively reduce these defects [71]. With suppressed iodide defects in the perovskite film. Uddin et al. [71] demonstrated perovskite films with enhanced photoluminescence performance and reduced deep-level trap concentration, in despite of a decrease in seed sizes. The use of zinc additive agents enables the fabrication of more cohesive perovskite layers over extensive-area (78–108 cm^2) using blade-coating technique. The fabrication process involves blade coating the PTAA layer, followed by blade coating the perovskite precursor ink, annealing, and deposition of additional layers. Submodules are created by performing laser scribing after copper electrode deposition, resulting in modules with 20 sub-cells. Regarding Figure 12, PSMs with addition of these additives achieve certified PCEs of 19.21% and 19.60% for aperture areas of 108 cm^2 and 84 cm^2, respectively.

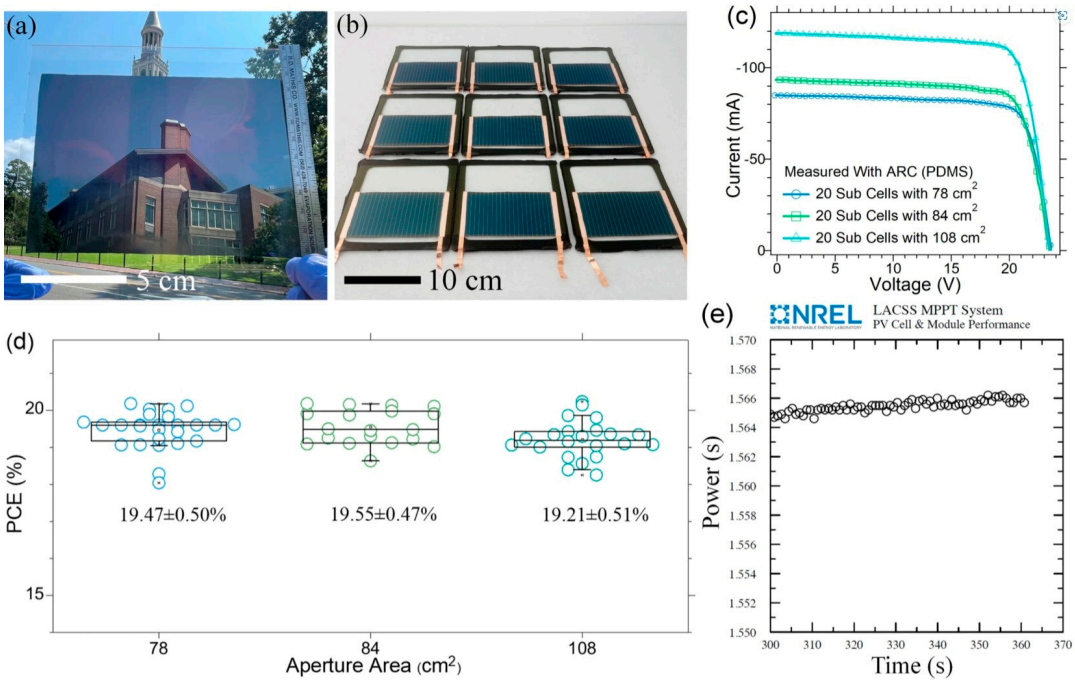

Figure 12. (**a**) An image of a blade-coated $FA_{0.3}MA_{0.7}PbI_3$ perovskite layer on an ITO substrate, covering around 130 cm^2, (**b**) A photograph showing enclosed minimodules with aperture areas of approximately 78 cm^2, (**c**) J-V plots illustrating the characteristics of minimodules with aperture areas of 78 cm^2, 84 cm^2, and 108 cm^2, respectively, (**d**) Performance of minimodule with various aperture areas, (**e**) Stable power output from the champion minimodules [71].

Through a meticulously designed and executed research endeavor, Wang et al. [72] have introduced a novel additive strategy for n-doping in p-i-n structured perovskite-based solar devices. This approach effectively overcomes the limitations posed by conventional n-dopants by intermingling 1-ethyl-3-methylimidazolium-2-carboxylate (EMIC) as n-dopant, which not only maintains the pristine crystallinity and morphology of the perovskite material but also remarkably prolongs the electron diffusion length. Leveraging the favorable solubility of EMIC in most polar solvents, the team has seamlessly integrated this n-dopant into the perovskite precursor solutions, enabling its efficient incorporation during the film production steps. Upon thermal annealing, the decarboxylation of EMIC releases the highly reactive imidazolylidene species, which efficiently donates electrons and increase conductivity, thereby enhancing the photovoltaic performance. With this groundbreaking n-doping strategy, the researchers have demonstrated outstanding PCE of 24.3% for blade-coated perovskite solar cells at device area of 7.4 mm^2. Remarkably, the large-area perovskite modules exhibit a mirror-like surface and excellent uniformity, attaining PCE of 20.6% at 25.0 cm^2 aperture areas, which further showcase the scalability and compatibility of this n-doping approach for PSM manufacturing.

The challenge of scalable production of high-efficiency all-perovskite tandem solar devices persists, primarily attributed to the pervasive issues of non-uniform crystallization, suboptimal concealed interfaces, and the small-bandgap sub cells comprising poor quality lead-tin perovskite layers. In this seminal investigation, the researchers have ingeniously used aminoacetamide hydrochloride (AAH) to selectively passivate defects and yield homogenization of perovskite crystallization at the critical buried interface. This strategic intervention has facilitated extension of the operating framework for the blade-coating of Pb-Sn perovskite layers. This additive approach has culminated in all-perovskite tandem solar modules that attained a certified performance of 24.5% over a 20.25 cm^2 aperture area, demonstrating an efficacious solution to the long-standing challenges of scalability [73].

In addition to additive method, another group addressed the challenge of all-perovskite tandem solar cells through the deployment of hybrid fullerenes (HF) as electron transport

layer, which is deposited via blade-coating for both top and bottom sub cells [74]. The hybrid fullerenes consisting of a synergistic blend of fullerene derivatives exhibits enhanced conductivity, reduced interfacial nonradiative recombination, and superior energy level alignment related to conventional thermally evaporated C_{60}. Leveraging this novel ETL approach, the researchers have fabricated all-perovskite tandem solar modules and attained champion efficiency of 23.3% over a 20.25 cm^2 aperture area, further advancing the manufacturing of low-cost, large-scale, and high-efficiency all-perovskite tandem solar modules.

More research and innovations on charge transporting layer have been conducted to advance blade coated PSMs. Ren et al. [75] developed a novel polymeric hole transport material (HTM), termed Poly-4PACz, through the polymerization of carbazole phosphonic acid (PACz). This versatile material exhibits capability of suppressing interfacial recombination, improved hole-extraction capacity, and enhanced HTM/perovskite interface. Crucially, Poly-4PACz demonstrates superior conductivity and wettability on both indium-doped tin oxide (ITO) and fluorine-doped tin oxide (FTO) substrates, enabling scalable coating of perovskite films without thickness sensitivity for device performance. Leveraging these desirable properties, the team fabricated high-performance blade-coated p-i-n PSCs and PSMs, achieving champion efficiency of 20.7% and 24.4% at 25.0 mm^2 and 6.84 cm^2 aperture areas, respectively.

The utilization of sputtered nickel oxide as an inorganic HTL in PSCs has garnered substantial interest because of its advantages of cost-effectiveness and robustness. However, the prevalent flaw is the suboptimal open-circuit voltage stemming from interface issues. Tutundzic et al. [76] used phosphonic acid self-assembled monolayers (SAMs) as interfacial layer to modulate the sputtered perovskite/NiO_x interface and assist hole extraction. The ultrathin SAM layer is blade coated. Along with addition of stabilizing agent, namely octadecyl 3-(3,5-di-tertbutyl-4-hydroxyphenyl)propionate (I-76), the performance of NiO_x/SAM-based PSCs has been enhanced, yielding a 21.8% PCE. Applying these strategies enabled upscaling of perovskite modules with efficiencies of 20.4%, 18.0%, and 16.4% for 4, 16, and 100 cm^2 aperture areas, respectively.

Flexible PSCs have garnered notable attention due to their promising prospects for soft light-weight applications. While the poor quality of the embedded perovskite-substrate interface, along with large deformation from flexible substrates, has significantly hindered the performance of these flexible devices. In this regard, Xu et al. [77] incorporated the organic compound, entinostat, into the hole extraction material, poly(bis(4-phenyl)(2,4,6-trimethylphenyl)amine) (PTAA) to improve bonding at the perovskite-ITO interface. The perovskite layer was formed using blade coating and applied on top of an elastic indium tin oxide base with PTAA as HTL. The multiple functional groups of entinostat incorporated in PTAA allow for effective interactions with both perovskites and indium tin oxide, significantly decreasing the gap density at the bottom of the perovskite layer. Consequently, the team demonstrated inverted limited-area (8 mm^2) bendable PSCs with an impressive efficiency of 23.4% and PCE of ~19% for mini-modules with aperture area of 9 cm^2.

The same to the printed PSCs, common strategies, such as solvent engineering and surface passivation, were also applied to PSM fabrication. Zhuang et al. [78] investigated the utilization of a new modifier, N,N-diphenylguanidine monohydrobromide (DPGABr), which is dissolved in acetonitrile (ACN) solvent, for the surface reconstruction of $MA_{0.7}FA_{0.3}PbI_3$ perovskite layer. The methodology involves the blade coating of DPGABr solution onto the perovskite surface in an ambient environment, resulting in the formation of a thin complex of DPGABr/PbI_2. This surface reconstruction enhances the performance of PSCs by passivating surface defects, inducing n-type doping, thereby facilitating electron transfer. The PSCs equipped with the reconstructed surface exhibit a notable 15% improvement in average performance. The maximum efficiency achieved through this novel surface reconstruction is 24.04%. Moreover, these devices demonstrate exceptional long-term reliability, with negligible efficiency decay even after a 1-year period of storage in ambient conditions.

Through strategic development of a meniscus-modulated blade coating scheme, along with solvent engineering, researchers have successfully addressed the key problems associated with the scalable production of formamidinium lead triiodide ($FAPbI_3$) perovskite layers [79]. By meticulously tailoring the film formation process, the team has achieved large-area $FAPbI_3$ films exhibiting exceptional characteristics, including preferred crystal orientation, enlarged grain sizes, excellent uniformity, and precisely controlled thickness—attributes that are pivotal for optimizing device performance. Leveraging this meniscus-modulated blade coating, Huang et al. [79] have demonstrated PCE of 25.31% for small-area cells (0.09 cm^2) and an impressive 23.34% for sizable minimodules (12.4 cm^2), which has been officially certified at 23.09%. Remarkably, these high-performing perovskite minimodules have also showcased exceptional long-term reliability, retaining over 93% of their primary performance even after 2000 h of rigorous open-air testing.

Zhang et al. [80] developed a specific solid–liquid two-step perovskite film generation method, combining the benefits of vapor deposition and solution processing. This innovative approach enabled generation of extensive-area perovskite films without utilization of noxious solvent, while accommodating substrates with disparate degrees of surface roughness. Furthermore, modification of the perovskite/NiO_x buried interface with incorporation of urea additives leveraged to mitigate interfacial recombination and regulate the perovskite crystallization process. The cumulative outcomes of these interventions include extensive-area perovskite films with enlarged grains, reduced defects, and diminished pinholes. The fabricated PSMs with an inverted architecture demonstrated a champion performance of 20.56% over remarkable effective area of 61.56 cm^2 and a significant enhancement in long-term stability. Overall, this solid–liquid two-step perovskite film generation method offers a compelling solution to the long-standing challenge of ensuring uniformity over large-area perovskite film by printing.

5.2. Notable PSMs Based on Slot Die Coating

Rana et al. [81] implemented additive engineering with $CsPbBr_3$ and KPb_2Br_5 alkali salts incorporated in the perovskite precursor ink to control and optimize perovskite crystallization. This material design enabled scalable slot-die coating fabrication of highly crystalline and homogeneous $Cs_{0.15}FA_{0.85}Pb(I_{0.83}\ Br_{0.17})_3$ (CsFA) perovskite films. The addition of alkali salts promoted nucleation at the perovskite/SnO_2 contact, leading to larger grains and improved optoelectronic properties. The slot-die coated champion PSCs with 0.09 cm^2 active area demonstrated highest PCE of 18.94% under 1 sun radiation. The methylammonium-free perovskite modules with an effective area of 57.5 cm^2 achieved efficiency of 16.22%. Notably, the unencapsulated modules retained 82% of its primary performance after 4800 h under 30% relative humidity. These results demonstrate the successful application of the seed-assisted crystallization approach and slot-die coating for extensive-scale manufacturing of high-performance and reliable PSCs and PSMs.

Sangale et al. [82] elucidated the pioneering employment of locally supersaturated perovskite ink (LSPI) approach for PSC assembly, a methodology befitting continuous roll-to-roll processing. Leveraging a single-solvent perovskite precursor ink, and judiciously incorporating a tiny quantity of a modulator, 1,2-dichlorobenzene (DCB), the researchers skillfully manipulated the rheological characteristics of the perovskite ink by lowering surface tension and improving the wetting capability to facilitate uniform wet film creation by slot-die coating (see Figure 13). Crucially, the addition of DCB molecules engendered the formation of perovskite seeds through heterogeneous nucleation at low free energy, thus enabled the growth of large and dense grains. Remarkably, this LSPI-based slot-die coating yielded PSCs with an impressive nominal performance of 20.61% for effective areas of 0.1 cm^2 and minimodules with PCE of 17.66% over an active area of 8.64 cm^2.

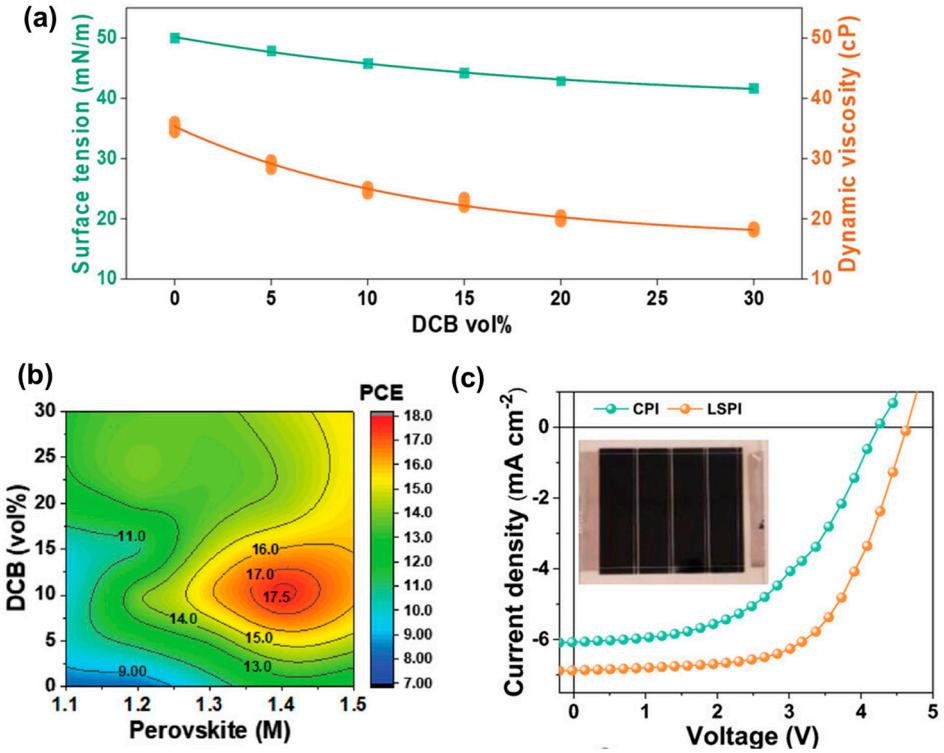

Figure 13. (**a**) Rheological characteristics of perovskite precursor inks modulated by DCB, (**b**) Visualizing PCE dependence on ink composition, (**c**) Performance characteristics of perovskite minimodule under standard testing conditions [82].

Wang et al. [83] addressed the detrimental chemical reactions that persistently occur at the buried interface between the sputtered nickel oxide hole transport layer (15–20 nm) and the $CH_3NH_3PbI_3$ perovskite absorber layer (300–350 nm) in inverted p-i-n configurations. By incorporating the multi-functional weakly acidic (pH 6.5) stabilizer, L-ascorbic acid (L-AA, 0.1 M) into the lead iodide (1.1 M) and methylammonium iodide (1.1 M) precursor solution, the authors could simultaneously suppress the chemical reactions at NiO_2/$MAPbI_3$ interface and stabilize the precursors, mitigating oxidation of iodide ions and deprotonation of organic cations. Attributed to improved crystallinity as indicated by XRD analysis and inhibition of undesired reactions at the buried layer as observed by UPS and XPS characterization, PSCs fabricated with this approach yield an impressive efficiency exceeding 22% (Voc: 1.19 V, Jsc: 24.48 mA cm^{-2}, FF: 79.5%) alongside prolonged stability. Notably, large-area (active area >50 cm^2) PSMs demonstrated with PCE of 19.17%. This study indicates that additive engineering can be an effective way to improve the quality of buried interface between sputtering deposited NiO^2 and perovskite absorber layer.

Subbiah et al. [84] focused on traditional $MAPbI_3$ perovskite-based PSCs with planar p-i-n configuration produced by anti-solvent-free slot-die coating. Key strategies such as solvent engineering, and surface passivation were employed, resulting in a remarkable performance of 21.8%. The research also extended the slot-die coating to develop silicon/perovskite monolithic 2-terminal tandem structures. By incorporating a textured silicon bottom cell and tuning the perovskite absorber 's band gap, a high PCE of 23.8% was obtained for the tandems, as indicated in Figure 14. Minimodules with effective area of 6.8 cm^2, consisting of four sub cells (1.7 cm^2 for each) were also demonstrated, yielding champion PCE of 14.4%.

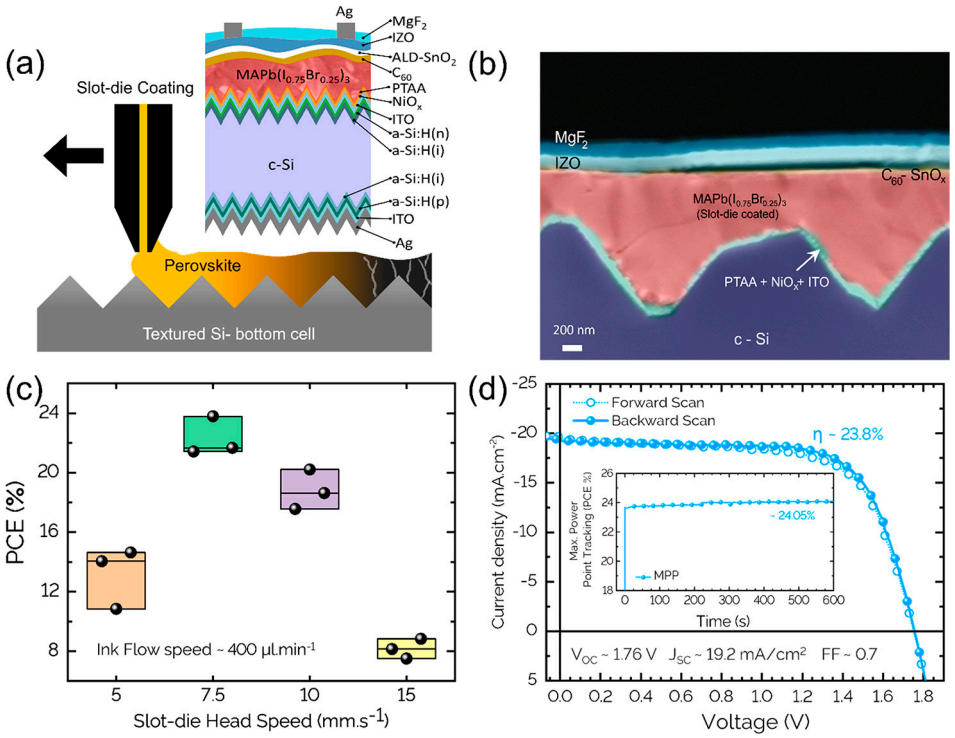

Figure 14. (**a**) Slot die coating deposition of a wide band gap perovskite absorber layer on textured silicon surface to make perovskite/silicon tandem devices, (**b**) SEM image showing cross-section of textured silicon/perovskite tandem device made by slot die coating, (**c**) PCE statistics for slot-die-coated tandems at various head speeds, (**d**) J-V plot of the best slot die coated silicon/perovskite tandem devices [84].

Rana et al. [85] utilized a hydrophobic all-organic salt, namely fluorinated anilinium benzylphosphonate (FABP), as a surface modifier for slot-die-coated perovskite films and has shown promising outcomes in enhancing their efficiency and long-term stability. By effectively binding to cation and anion vacancies, the FABP organic salt plays as a molecular lock, reducing the access of external species and suppressing the release of volatile components. Extensive-area slot die coated PSMs treated with the surface modifier achieved the maximum working performance of 19.28%, and 17.62% for effective area of 58.5 cm^2 and aperture area of 64 cm^2, respectively. Remarkably, exposed mini modules, containing the organic surface modifier retained approximately 80% performance after 313 days under 30% relative humidity. Moreover, they exhibited over 90% of the primary operating efficiency for more than 850 h during the continuous MPPT measurement. These findings highlight the significant improvement in reliability and extended performance of slot die coated PSMs achieved with the all-organic surface modifier.

Li et al. [86] focused on developing large-area formamidinium lead triiodide ($FAPbI_3$) based PSC prototypes and outdoor stability testing. They employed a slot-die coating technique to deposit $FAPbI_3$ perovskite films on large areas and address ribbing issue by altering the rheological characteristics of the precursor solution based on 2-methoxyethanol (2ME). By adding acetonitrile (ACN) as a co-solvent to the precursor inks, they achieved smooth and high-quality perovskite layers. The optimized precursor ink composition, containing 46% volume of ACN, resulted in a certified efficiency of 22.3% for small-area solar cells. Figure 15b demonstrated scalability by fabricating series-interconnected mini-modules with PCEs exceeding 17% for PSMs with active area of 12.7 cm^2. The solar cell structure included indium tin oxide (ITO) substrate, MeO-2PACz as hole-transporting material, $FAPbI_3$ perovskite absorber, lithium fluoride (LiF), fullerene (C_{60}), SnO_2 replacing bathocuproine (BCP) for long lifespan, and copper (Cu). Encapsulated PSMs with

above architecture demonstrated superior stability, maintaining almost 100% of their initial efficiency over winter and spring seasons in field testing under continuous MTTP tracking.

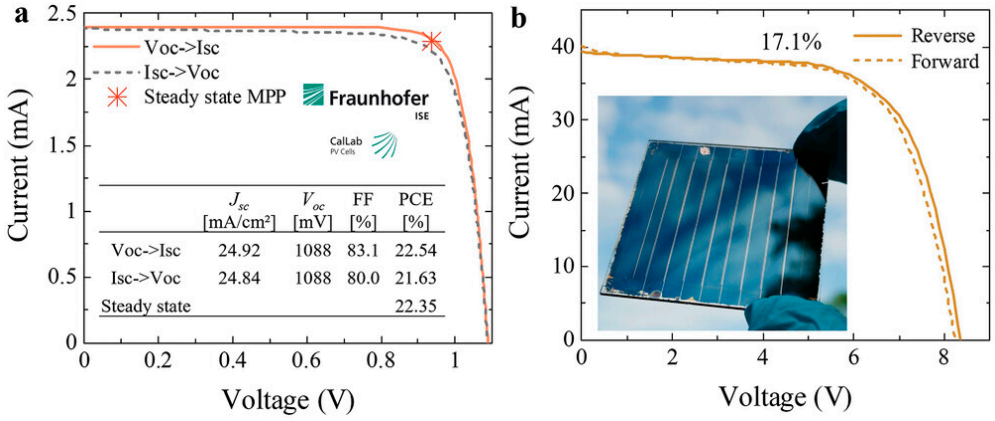

Figure 15. (**a**) Certified J-V plots of the top PSCs using Me-4PACz as HTL (**b**) J-V plots of a 25 cm^2 mini-module [86].

5.3. Notable PSMs Based on Screen Printing

Worsley et al. [87] focused on characterizing the defects related to TiO_2 infiltration in the manufacturing of mesoporous layer-based solar cells (MPSCs) and modules (MPSMs). The solar cell structure includes three screen-printed mesoporous films: TiO_2, ZrO_2, and carbon. The TiO_2 layer is key for achieving optimum operational performance and reproducibility. The study identifies and addresses specific defects in TiO_2 infiltration caused by issues namely, contaminant damage, mesh marking, environmental fluctuation, and printing problems. The study provides possible reasons and potential solutions for issues, serving as a valuable troubleshooting guide for improving the infiltration process in both research and large-scale manufacturing contexts.

Potts et al. [88] improved the performance of carbon-based mesoscopic PSMs by optimizing ink rheology for attaining high-quality TiO_2 with large-area screen printing. Inks with titanium dioxide nanoparticles (20 nm) and viscosities ranging from 30–150 Pa·s at a shear rate of $10s^{-1}$, which were varied by diluting the pastes with ethanol or ethyl cellulose, were assessed using high-speed imaging at 500 frames/s. Visualization elucidated that decreasing viscosity below 100Pa·s mitigates jetting instabilities during screen printing deposition, yielding mesostructured titanium dioxide films (150 nm) with superior topography (surface roughness <50 nm) and homogeneous infiltration of the methylammonium lead iodide ($MAPbI_3$) perovskite precursor solution (2.1M). At the optimal paste to dilutant ratio of 1:0.75, PSCs (0.1 cm^2) and scaled PSMs (224 cm^2) accomplished the best performance as substantiated by augmented open-circuit voltage and fill factor due to enhanced charge transport and collection.

In this study, Srisamran et al. evaluated the impact of ternary additives on the reliability and working efficiency of $MAPbI_3$-based MPSCs and PSMs [89]. The optimal composition of thiourea (TU), guanidinium thiocyanate (GT), and urea (U) additives resulted in impressive outcomes for enhancement of device performance. Fully screen-printed PSCs achieved a remarkable PCE of 16.40% with an effective area of 1 cm^2, significantly greater than pristine devices without ternary additives. Moreover, the PSMs exhibited a performance of 11.60% with an overall active area of about 51.50 cm^2, more than three times higher than PSMs without additives. Notably, both PSCs and PSMs demonstrated excellent stability over extended periods. These findings stress the potential of ternary additives for accomplishing high-quality films by screen printing, paving the way for mass production of PSMs and commercialization of perovskite-based solar technology.

As a summary, Figure 16 shows the PSC and PSM performance over various coating areas by blade coating, slot die coating, and screen printing, and Table 2 lists additional high-performance printed PSMs.

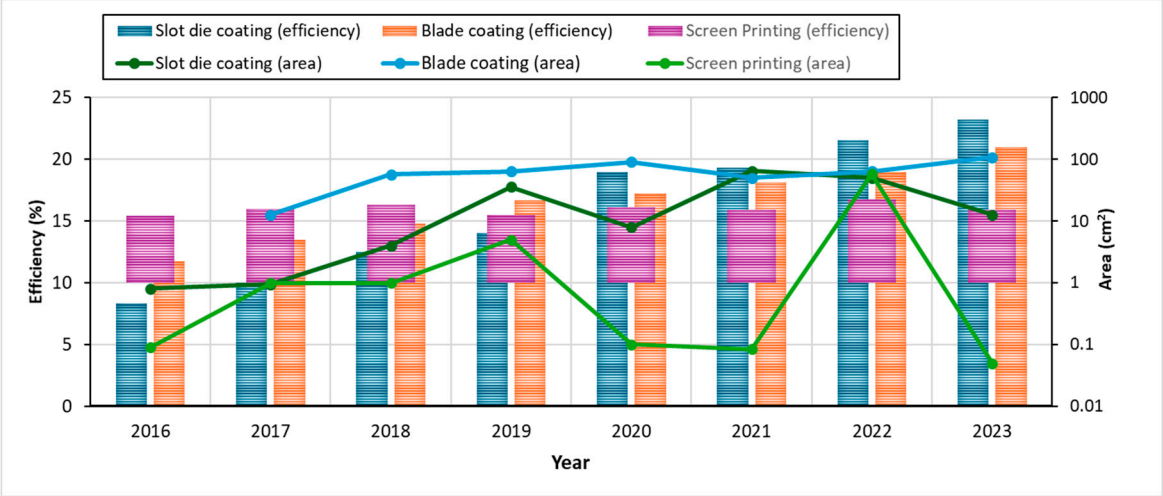

Figure 16. Performance development of PSMs with various unit areas, in terms of different printing methods [90].

Table 2. Additional high-performance perovskite solar modules by printing.

Cell Design	Deposition Approaches			Area (cm^2)	PCE (%)	Ref.
NIP structure	Perovskite	HTL	ETL			
Glass material/ITO/$cTiO_2$/$CH_3NH_3PbI_3$/Spiro-OMeTAD/Au	Slot die coating	Slot die coating	Physical Vapor Deposition	168.75	11	[91]
Glass material/FTO/$cTiO_2$/$mTiO_2$/(FA1 − x-yMA_xCsy)Pb (I1 − xBrx)$_3$/Spiro-OMeTAD/Au	Blade coating	Spin coating	Spray/Blade coating	50	11.6	[92]
Glass material/FTO/$cTiO_2$/$mTiO_2$/$CH_3NH_3PbI_3$/carbon-based layer	Inkjet coating	Screen printing	Inkjet coating	52.4	10.07	[93]
Glass material/FTO/SnO_2/$CH_3NH_3PbI_3$/Spiro-OMeTAD/Au	Spin coating	Blade coating	Spin coating	13.8	13.1	[94]
Glass material/FTO/SnO_2/$CH_3NH_3PbI_3$/Spiro-OMeTAD/Au	Spin coating	Blade coating	Chemical vapor deposition	53.64	17.82	[95]
ITO/PET/SnO_2/$Cs_{0.05}(FA_{0.85}MA_{0.15})_{0.95}Pb(I_{0.85}Br_{0.15})_3$/Spiro-OMeTAD/Au	Spin coating	Spin coating	Slot die coating	14.89	16.07	[96]
PEDOT:PSS/$FA_{0.7}MA_{0.3}PbI_{0.5}Sn_{0.5}I_3$/$C_{60}$/$SnO_2$/Ag	Blade coating	Blade coating	Vapor transport deposition	21.7	20.25	[97]
Glass material/ITO/NiO/VNPB/$Cs_{0.35}FA_{0.65}PbI_{1.8}Br_{1.2}$/$C_{60}$/$SnO_2$/Au	Blade coating	Blade coating	Vapor transport deposition	21.7	20.25	
Glass material/FTO/NiMgLiO/$FA_{0.83}Cs_{0.17}(PbI_2)_{0.83}Br_{0.17}$/LiF/$C_{60}$/BCP/Bi/Ag	Slot die coating	Vapor transport deposition	Vapor transport deposition	16.63	20.77	[98]

6. Conclusions and Outlook

This review focuses on state-of-the-art high-performance PSCs and PSMs fabricated by printing techniques, particularly, screen printing, slot die coating, and blade coating, because of their widely applications in manufacturing of perovskite-based photovoltaic devices. This discerning selection is grounded in a rigorous analysis of critical parameters encompassing film quality, device efficiency and stability, and printing scalability and cost-effectiveness. Screen printing is distinguished by its intrinsic simplicity and scalability, facilitating the rapid and large-scale deposition of thick films. Recent reviews elucidate that this technique adeptly balances production velocity with material utilization [99,100]. Conversely, slot die coating has capability of precise control over film thickness and uniformity over large area, optimizing material consumption while enabling high-speed, large-area deposition. The printing phenomena and film quality are governed by fundamental fluid

dynamics, as the rheological characteristics of the ink play a critical role in printing setting, which needs to be meticulously manipulated to achieve the desired film attributes. Similarly, blade coating (or doctor blade coating) confers exceptional command over film thickness and uniformity, rendering it particularly suitable for deposition of ultra-thin films. Its economic viability and scalability further enhance its appeal, as highlighted in the existing literature [101,102].

In each printing technique section, high performance PSCs and PSMs are also grouped based on the methodologies used to improve the efficiency and stability, as well as film quality. The common strategies used to enhance performance of small-area and usually spin-coated devices are also employed on printed PSCs and PSMs. These strategies include additive, solvent engineering, surface passivation, interfacial engineering (including novel electron and hole transporting materials). As additive, novel charge transporting materials, and/or solvent engineering does not add extra layer for printing, these strategies could be favorably considered in cost-effective, mass production of PSMs. Moreover, some schemes that are specifically designed to high-speed printing for improved film quality and uniformity over large area were also examined in this review. As perovskite-based photovoltaic devices include multiple stacking layers, some films are relatively thick in a few hundred of nanometers or microns, such as perovskite absorber or solution-processed carbon or silver paste electrode, which is suitable for slot die coating and screen printing, and some layers have to be extremely thin in tens of nanometers, such as charge transporting layer interfacial engineering film, or surface passivation layer, which is appropriate for blade coating, the integration of hybrid printing techniques could be an effective and compelling avenue for commercial scalability. By harnessing the distinctive advantages of slot die coating, screen printing, and blade coating, large-scale, cost-effective manufacturing of high-performance perovskite solar cells and modules can be actualized. Along with scientific advancement in materials of each stacking layer and device architecture, perovskite-based photovoltaics could surmount current stability and lifespan challenges, becoming a cornerstone solar technology that will be broadly adopted in the future market.

Funding: This material is based upon work supported by the U.S. Department of Energy's Office of Energy Efficiency and Renewable Energy (EERE) Solar Energy Technologies Office (SETO) under the SIPS Award Number DE-EE0010242. This work was also partially supported by the National Science Foundation under the grant ECCS-2053954. Dawen Li acknowledges financial support for Shohreh Soltani from Graduate Council Fellowship (GCF) at The University of Alabama.

Conflicts of Interest: The authors declare no conflict of interest.

References

1. Kojima, A.; Teshima, K.; Shirai, Y.; Miyasaka, T. Organometal halide perovskites as visible-light sensitizers for photovoltaic cells. *J. Am. Chem. Soc.* **2009**, *131*, 6050–6051. [CrossRef]
2. Zhao, Y.; Ma, F.; Qu, Z.; Yu, S.; Shen, T.; Deng, H.X.; Chu, X.; Peng, X.; Yuan, Y.; Zhang, X.; et al. Inactive $(PbI_2)_2RbCl$ stabilizes perovskite films for efficient solar cells. *Science* **2022**, *377*, 531–534. [CrossRef] [PubMed]
3. Li, X.; Zhang, W.; Guo, X.; Lu, C.; Wei, J.; Fang, J. Constructing heterojunctions by surface sulfidation for efficient inverted perovskite solar cells. *Science* **2022**, *375*, 434–437. [CrossRef] [PubMed]
4. Wang, J.; Bi, L.; Huang, X.; Feng, Q.; Liu, M.; Chen, M.; An, Y.; Jiang, W.; Lin, F.R.; Fu, Q.; et al. Bilayer interface engineering through 2D/3D perovskite and surface dipole for inverted perovskite solar modules. *eScience* **2024**, *4*, 100308. [CrossRef]
5. Wang, J.; Bi, L.; Fu, Q.; Jen, A.K. Methods for Passivating Defects of Perovskite for Inverted Perovskite Solar Cells and Modules. *Adv. Energy Mater.* **2024**, *14*, 2401414. [CrossRef]
6. Hutter, E.M.; Eperon, G.E.; Stranks, S.D.; Savenije, T.J. Charge carriers in planar and meso-structured organic–inorganic perovskites: Mobilities, lifetimes, and concentrations of trap states. *J. Phys. Chem. Lett.* **2015**, *6*, 3082–3090. [CrossRef] [PubMed]
7. De Wolf, S.; Holovsky, J.; Moon, S.-J.; Löper, P.; Niesen, B.; Ledinsky, M.; Haug, F.-J.; Yum, J.-H.; Ballif, C. Organometallic Halide Perovskites: Sharp Optical Absorption Edge and Its Relation to Photovoltaic Performance. *J. Phys. Chem. Lett.* **2014**, *5*, 1035–1039. [CrossRef]
8. Yin, W.J.; Shi, T.; Yan, Y. Unique properties of halide perovskites as possible origins of the superior solar cell performance. *Adv. Mater.* **2014**, *26*, 4653–4658. [CrossRef] [PubMed]

9. Miyata, A.; Mitioglu, A.; Plochocka, P.; Portugall, O.; Wang, J.T.-W.; Stranks, S.D.; Snaith, H.J.; Nicholas, R.J. Direct measurement of the exciton binding energy and effective masses for charge carriers in organic–inorganic tri-halide perovskites. *Nat. Phys.* **2015**, *11*, 582–587. [CrossRef]
10. Saliba, M.; Correa-Baena, J.; Graetzel, M.; Hagfeldt, A.; Abate, A. Perovskite solar cells: From the atomic level to film quality and device performance. *Angew. Chem. Int. Ed.* **2018**, *57*, 2554–2569. [CrossRef] [PubMed]
11. Castriotta, L.A.; Zendehdel, M.; Nia, N.Y.; Leonardi, E.; Löffler, M.; Paci, B.; Generosi, A.; Rellinghaus, B.; Di Carlo, A. Reducing losses in perovskite large area solar technology: Laser design optimization for highly efficient modules and minipanels. *Adv. Energy Mater.* **2022**, *12*, 2103420. [CrossRef]
12. Zhu, K.; Lu, Z.; Cong, S.; Cheng, G.; Ma, P.; Lou, Y.; Ding, J.; Yuan, N.; Rümmeli, M.H.; Zou, G. Ultraflexible and lightweight bamboo-derived transparent electrodes for perovskite solar cells. *Small* **2019**, *15*, 1902878. [CrossRef]
13. Chu, L.; Zhai, S.; Ahmad, W.; Zhang, J.; Zang, Y.; Yan, W.; Li, Y. High-performance large-area perovskite photovoltaic modules. *Nano Res. Energy* **2022**, *1*, 9120024. [CrossRef]
14. Gusain, A.; Thankappan, A.; Thomas, S. Roll-to-roll printing of polymer and perovskite solar cells: Compatible materials and processes. *J. Mater. Sci.* **2020**, *55*, 13490–13542. [CrossRef]
15. Dou, B.; Whitaker, J.B.; Bruening, K.; Moore, D.T.; Wheeler, L.M.; Ryter, J.; Breslin, N.J.; Berry, J.J.; Garner, S.M.; Barnes, F.S.; et al. Roll-to-Roll Printing of Perovskite Solar Cells. *ACS Energy Lett.* **2018**, *3*, 2558–2565. [CrossRef]
16. Elangovan, N.K.; Kannadasan, R.; Beenarani, B.B.; Alsharif, M.H.; Kim, M.K.; Inamul, Z.H. Recent developments in perovskite materials, fabrication techniques, band gap engineering, and the stability of perovskite solar cells. *Energy Rep.* **2024**, *11*, 1171–1190. [CrossRef]
17. Wang, Y.; Duan, C.; Lv, P.; Ku, Z.; Lu, J.; Huang, F.; Cheng, Y.-B. Printing strategies for scaling-up perovskite solar cells. *Natl. Sci. Rev.* **2021**, *8*, nwab075. [CrossRef] [PubMed]
18. Peng, Y.; Cheng, Y.; Wang, C.; Zhang, C.; Xia, H.; Huang, K.; Tong, S.; Hao, X.; Yang, J. Fully doctor-bladed planar heterojunction perovskite solar cells under ambient condition. *Org. Electron.* **2018**, *58*, 153–158. [CrossRef]
19. Kim, B.; Ko, S.G.; Sonu, K.S.; Ri, J.H.; Kim, U.C.; Ryu, G.I. Effects of Adding PbI2 on the Performance of Hole-Transport Material-Free Mesoscopic Perovskite Solar Cells with Carbon Electrode. *J. Electron. Mater.* **2018**, *47*, 6266–6271. [CrossRef]
20. Patidar, R.; Burkitt, D.; Hooper, K.; Richards, D.; Watson, T. Slot-die coating of perovskite solar cells: An overview. *Mater. Today Commun.* **2019**, *22*, 100808. [CrossRef]
21. Krebs, F.C. Fabrication and processing of polymer solar cells: A review of printing and coating techniques. *Sol. Energy Mater. Sol. Cells* **2009**, *93*, 394–412. [CrossRef]
22. Schmidt, T.M.; Larsen-Olsen, T.T.; Carlé, J.E.; Angmo, D.; Krebs, F.C. Upscaling of perovskite solar cells: Fully ambient roll processing of flexible perovskite solar cells with printed back electrodes. *Adv. Energy Mater.* **2015**, *5*, 1500569. [CrossRef]
23. Mathies, F.; Eggers, H.; Richards, B.S.; Hernandez-Sosa, G.; Lemmer, U.; Paetzold, U.W. Inkjet-printed triple cation perovskite solar cells. *ACS Appl. Energy Mater.* **2018**, *1*, 1834–1839. [CrossRef]
24. Rong, Y.; Ming, Y.; Ji, W.; Li, D.; Mei, A.; Hu, Y.; Han, H. Toward industrial-scale production of perovskite solar cells: Screen printing, slot-die coating, and emerging techniques. *J. Phys. Chem. Lett.* **2018**, *9*, 2707–2713. [CrossRef] [PubMed]
25. Kim, Y.Y.; Yang, T.Y.; Suhonen, R.; Välimäki, M.; Maaninen, T.; Kemppainen, A.; Jeon, N.J.; Seo, J. Gravure-printed flexible perovskite solar cells: Toward roll-to-roll manufacturing. *Adv. Sci.* **2019**, *6*, 1802094. [CrossRef]
26. Bishop, J.E.; Routledge, T.J.; Lidzey, D.G. Advances in spray-cast perovskite solar cells. *J. Phys. Chem. Lett.* **2018**, *9*, 1977–1984. [CrossRef] [PubMed]
27. Siegrist, S.; Pious, J.K.; Lai, H.; Kothandaraman, R.K.; Luo, J.; Vlnieska, V.; Tiwari, A.N.; Fu, F. Stabilizing Solution–Substrate Interaction of Perovskite Ink on PEDOT:PSS for Scalable Blade Coated Narrow Bandgap Perovskite Solar Modules by Gas Quenching. *Sol. RRL* **2024**, *8*, 2400447. [CrossRef]
28. Duarte, V.C.M.; Andrade, L. Recent Advancements on Slot-Die Coating of Perovskite Solar Cells: The Lab-to-Fab Optimisation Process. *Energies* **2024**, *17*, 3896. [CrossRef]
29. Chen, C.; Ran, C.; Yao, Q.; Wang, J.; Guo, C.; Gu, L.; Han, H.; Wang, X.; Chao, L.; Xia, Y.; et al. Screen-Printing Technology for Scale Manufacturing of Perovskite Solar Cells. *Adv. Sci.* **2023**, *10*, 2303992. [CrossRef]
30. Ouedraogo, N.A.N.; Ouyang, Y.; Guo, B.; Xiao, Z.; Zuo, C.; Chen, K.; He, Z.; Odunmbaku, G.O.; Ma, Z.; Long, W.; et al. Printing Perovskite Solar Cells in Ambient Air: A Review. *Adv. Energy Mater.* **2024**, *14*, 2401463. [CrossRef]
31. Bishop, J.E.; Smith, J.A.; Lidzey, D.G. Development of spray-coated perovskite solar cells. *ACS Appl. Mater. Interfaces* **2020**, *12*, 48237–48245. [CrossRef] [PubMed]
32. Jia, P.; Chen, G.; Li, G.; Liang, J.; Guan, H.; Wang, C.; Pu, D.; Ge, Y.; Hu, X.; Cui, H.; et al. Intermediate Phase Suppression with Long Chain Diammonium Alkane for High Performance Wide-Bandgap and Tandem Perovskite Solar Cells. *Adv. Mater.* **2024**, *36*, 2400105. [CrossRef]
33. Zhang, D.; Khasnabis, S.; Wang, W.; Yeddu, V.; Moradi, S.; Awais, M.; Nguyen, H.D.; Reinecke, S.B.; Haruta, Y.; Godin, R.; et al. Cadmium-Doping Slows Trap Emptying in Ambient-Air Blade-Coated Formamidinium Lead Iodide Perovskite Solar Cells. *Adv. Energy Mater.* **2024**, *14*, 2303858. [CrossRef]
34. Zhu, H.; Shao, B.; Yin, J.; Shen, Z.; Wang, L.; Huang, R.; Chen, B.; Wehbe, N.; Ahmad, T.; Abulikemu, M.; et al. Retarding Ion Migration for Stable Blade-Coated Inverted Perovskite Solar Cells. *Adv. Mater.* **2023**, *36*, 2306466. [CrossRef] [PubMed]

35. Shi, X.; Liu, T.; Dou, Y.; Hu, X.; Liu, Y.; Wang, F.; Wang, L.; Ren, Z.; Chen, S. Air-Processed Perovskite Solar Cells with >25% Efficiency and High Stability Enabled by Crystallization Modulation and Holistic Passivation. *Adv. Mater.* **2024**, *36*, 2402785. [CrossRef] [PubMed]
36. Du, Y.; Tian, Q.; Wang, S.; Yin, L.; Ma, C.; Wang, Z.; Lang, L.; Yang, Y.; Zhao, K.; Liu, S. Crystallization Control Based on the Regulation of Solvent–Perovskite Coordination for High-Performance Ambient Printable $FAPbI_3$ Perovskite Solar Cells. *Adv. Mater.* **2023**, *36*, 2307583. [CrossRef] [PubMed]
37. Pu, D.; Zhou, S.; Guan, H.; Jia, P.; Chen, G.; Fang, H.; Fu, S.; Wang, C.; Hushvaktov, H.; Jumabaev, A.; et al. Enhancing Efficiency and Intrinsic Stability of Large-Area Blade-Coated Wide-Bandgap Perovskite Solar Cells Through Strain Release. *Adv. Funct. Mater.* **2024**, *34*, 2314349. [CrossRef]
38. Subbiah, A.S.; Merino, L.V.T.; Pininti, A.R.; Hnapovskyi, V.; Mannar, S.; Aydin, E.; Razzaq, A.; Allen, T.G.; De Wolf, S. Enhancing the Performance of Blade-Coated Perovskite/Silicon Tandems via Molecular Doping and Interfacial Energy Alignment. *ACS Energy Lett.* **2024**, *9*, 727–731. [CrossRef]
39. Liang, J.; Du, D.; Gao, C.; Qiao, F.; He, L.; Zhang, D.; Bao, J.; Liu, H.; Shen, W. Controllable Cosolvent Blade-Coating Strategy toward Low-Temperature Fabrication of Perovskite Solar Cells. *ACS Appl. Energy Mater.* **2023**, *6*, 10842–10852. [CrossRef]
40. Mariotti, S.; Köhnen, E.; Scheler, F.; Sveinbjörnsson, K.; Zimmermann, L.; Piot, M.; Yang, F.; Li, B.; Warby, J.; Musiienko, A.; et al. Interface engineering for high-performance, triple-halide perovskite–silicon tandem solar cells. *Science* **2023**, *381*, 63–69. [CrossRef] [PubMed]
41. Chen, S.; Dai, X.; Xu, S.; Jiao, H.; Zhao, L.; Huang, J. Stabilizing perovskite-substrate interfaces for high-performance perovskite modules. *Science* **2021**, *373*, 902–907. [CrossRef] [PubMed]
42. Wang, F.F.; Liu, T.X.; Cui, Z.W.; Wang, L.Y.; Dou, Y.J.; Shi, X.Y.; Luo, S.W.; Hu, X.D.; Ren, Z.J.; Liu, Y.Y.; et al. Simplified pin perovskite solar cells with a multifunctional polyfullerene electron transporter. *Chin. J. Polym. Sci.* **2024**, *42*, 1060–1066. [CrossRef]
43. Yang, G.; Yu, Z.J.; Wang, M.; Shi, Z.; Ni, Z.; Jiao, H.; Fei, C.; Wood, A.; Alasfour, A.; Chen, B.; et al. Shunt mitigation toward efficient large-area perovskite-silicon tandem solar cells. *Cell Rep. Phys. Sci.* **2023**, *4*, 101628. [CrossRef]
44. Xu, K.; Al-Ashouri, A.; Peng, Z.W.; Köhnen, E.; Hempel, H.; Akhundova, F.; Marquez, J.A.; Tockhorn, P.; Shargaieva, O.; Ruske, F.; et al. Slot-die coated triple-halide perovskites for efficient and scalable perovskite/silicon tandem solar cells. *ACS Energy Lett.* **2022**, *7*, 3600–3611. [CrossRef] [PubMed]
45. Xu, F.; Liu, J.; Subbiah, A.S.; Liu, W.; Kang, J.; Harrison, G.T.; Yang, X.; Isikgor, F.H.; Aydin, E.; De Bastiani, M.; et al. Potassium thiocyanate-assisted enhancement of slot-die-coated perovskite films for high-performance solar cells. *Small Sci.* **2021**, *1*, 2000044. [CrossRef]
46. Li, J.; Dagar, J.; Shargaieva, O.; Flatken, M.A.; Köbler, H.; Fenske, M.; Schultz, C.; Stegemann, B.; Just, J.; Többens, D.M.; et al. 20.8% slot-die coated MAPbI3 perovskite solar cells by optimal DMSO-content and age of 2-ME based precursor inks. *Adv. Energy Mater.* **2021**, *11*, 2003460. [CrossRef]
47. Abate, S.Y.; Yang, Z.; Jha, S.; Ma, G.; Ouyang, Z.; Zhang, H.; Muhammad, S.; Pradhan, N.; Gu, X.; Patton, D.; et al. Room temperature slot-die coated perovskite layer modified with sulfonyl-γ-AApeptide for high performance perovskite solar devices. *Chem. Eng. J.* **2022**, *457*, 141199. [CrossRef]
48. Rana, T.R.; Abbas, M.; Schwartz, E.; Jiang, F.; Yaman, M.Y.; Xu, Z.; Ginger, D.S.; MacKenzie, D. Scalable Passivation Strategies to Improve Efficiency of Slot Die-Coated Perovskite Solar Cells. *ACS Energy Lett.* **2024**, *9*, 1888–1894. [CrossRef]
49. Zimmermann, I.; Harada, N.; Guillemot, T.; Aider, C.; Salim, K.M.M.; Nguyen, V.S.; Castillon, J.; Provost, M.; Medjoubi, K.; Cacovich, S.; et al. Slot-Die Deposition of CuSCN Using Asymmetric Alkyl Sulfides as Cosolvent for Low-Cost and Fully Scalable Perovskite Solar Cell Fabrication. *Sol. RRL* **2024**, *8*, 2400064. [CrossRef]
50. Sheng, J.; Zhu, X.; Xu, X.; He, J.; Ma, D.; Liu, J.; Wu, W. EtOH/H_2O ratio modulation on carbon for high-V_{oc} (1.03 V) printable mesoscopic perovskite solar cells without any passivation. *Mater. Adv.* **2023**, *4*, 1534–1545. [CrossRef]
51. Chen, C.; Chen, J.; Han, H.; Chao, L.; Hu, J.; Niu, T.; Dong, H.; Yang, S.; Xia, Y.; Chen, Y.; et al. Perovskite solar cells based on screen-printed thin films. *Nature* **2022**, *612*, 266–271. [CrossRef]
52. Chen, C.; Ran, C.; Guo, C.; Yao, Q.; Wang, J.; Niu, T.; Li, D.; Chao, L.; Xia, Y.; Chen, Y. Fully Screen-Printed Perovskite Solar Cells with 17% Efficiency via Tailoring Confined Perovskite Crystallization within Mesoporous Layer. *Adv. Energy Mater.* **2023**, *13*, 2302654. [CrossRef]
53. Zhu, W.; Wang, D.; Chen, Y.; Tao, Y.; Guo, R.; Zhang, Z.; Huang, Y.; Xiong, J.; Xiang, D.; Zhang, J. Room-Temperature Processed Annealing-Free Printable Carbon-Based Mesoscopic Perovskite Solar Cells with 17.34% Efficiency. *ACS Appl. Mater. Interfaces* **2024**, *16*, 7265–7274. [CrossRef] [PubMed]
54. He, J.; He, J.; Ma, D.; Sheng, J.; Shao, W.; Ding, T.; Wu, W. Competitive Formation Mechanism for Bidentate Passivation of Halogen Vacancies in Perovskite Based on 6-Chloropurine. *Small* **2023**, *20*, 2305127. [CrossRef] [PubMed]
55. Wang, L.; Xiong, J.; Wang, D.; Chen, Y.; Zhang, Y.; Wu, C.; Zhang, Z.; Wang, J.; Huang, Y.; Zhang, J. Efficient and stable full-printed mesoscopic perovskite solar cells with potassium hexafluorophosphate additives. *Sustain. Energy Fuels* **2023**, *7*, 2349–2356. [CrossRef]
56. Green, M.; Dunlop, E.; Hohl-Ebinger, J.; Yoshita, M.; Kopidakis, N.; Hao, X. Solar cell efficiency tables (version 57). *Prog. Photovolt. Res. Appl.* **2021**, *29*, 3–15. [CrossRef]
57. Khorasani, A.; Mohamadkhani, F.; Marandi, M.; Luo, H.; Abdi-Jalebi, M. Opportunities, Challenges, and Strategies for Scalable Deposition of Metal Halide Perovskite Solar Cells and Modules. *Adv. Energy Sustain. Res.* **2024**, *5*, 2300275. [CrossRef]

58. Scarpulla, M.A.; McCandless, B.; Phillips, A.B.; Yan, Y.; Heben, M.J.; Wolden, C.; Xiong, G.; Metzger, W.K.; Mao, D.; Krasikov, D.; et al. CdTe-based thin film photovoltaics: Recent advances, current challenges and future prospects. *Sol. Energy Mater. Sol. Cells* **2023**, *255*, 112289. [CrossRef]
59. Powalla, M.; Paetel, S.; Hariskos, D.; Wuerz, R.; Kessler, F.; Lechner, P.; Wischmann, W.; Friedlmeier, T.M. Advances in cost-efficient thin-film photovoltaics based on Cu (In, Ga) Se2. *Engineering* **2017**, *3*, 445–451. [CrossRef]
60. Li, Z.; Klein, T.R.; Kim, D.H.; Yang, M.; Berry, J.J.; van Hest, M.F.A.M.; Zhu, K. Scalable fabrication of perovskite solar cells. *Nat. Rev. Mater.* **2018**, *3*, 18017. [CrossRef]
61. Wang, F.; Bai, S.; Tress, W.; Hagfeldt, A.; Gao, F. Defects engineering for high-performance perovskite solar cells. *npj Flex. Electron.* **2018**, *2*, 22.
62. Szabó, G.; Park, N.-G.; De Angelis, F.; Kamat, P.V. Are Perovskite Solar Cells Reaching the Efficiency and Voltage Limits? *ACS Energy Lett.* **2023**, *8*, 3829–3831. [CrossRef]
63. Weerasinghe, H.C.; Macadam, N.; Kim, J.E.; Sutherland, L.J.; Angmo, D.; Ng, L.W.; Scully, A.D.; Glenn, F.; Chantler, R.; Chang, N.L.; et al. The first demonstration of entirely roll-to-roll fabricated perovskite solar cell modules under ambient room conditions. *Nat. Commun.* **2024**, *15*, 1656. [CrossRef] [PubMed]
64. Vesce, L.; Stefanelli, M.; Rossi, F.; Castriotta, L.A.; Basosi, R.; Parisi, M.L.; Sinicropi, A.; Di Carlo, A. Perovskite solar cell technology scaling-up: Eco-efficient and industrially compatible sub-module manufacturing by fully ambient air slot-die/blade meniscus coating. *Prog. Photovolt. Res. Appl.* **2024**, *32*, 115–129. [CrossRef]
65. Ren, Y.; Zhang, K.; Lin, Z.; Wei, X.; Xu, M.; Huang, X.; Chen, H.; Yang, S. Long-chain gemini surfactant-assisted blade coating enables large-area carbon-based perovskite solar modules with record performance. *Nano-Micro Lett.* **2023**, *15*, 182. [CrossRef]
66. Burkitt, D.; Patidar, R.; Greenwood, P.; Hooper, K.; McGettrick, J.; Dimitrov, S.; Colombo, M.; Stoichkov, V.; Richards, D.; Beynon, D.; et al. Roll-to-roll slot-die coated P–I–N perovskite solar cells using acetonitrile based single step perovskite solvent system. *Sustain. Energy Fuels* **2020**, *4*, 3340–3351. [CrossRef]
67. Teixeira, C.; Fuentes-Pineda, R.; Andrade, L.; Mendes, A.; Forgács, D. Fabrication of low-cost and flexible perovskite solar cells by slot-die coating for indoor applications. *Mater. Adv.* **2023**, *4*, 3863–3873. [CrossRef]
68. Li, C.-F.; Huang, H.-C.; Huang, S.-H.; Hsiao, Y.-H.; Chaudhary, P.; Chang, C.-Y.; Tsai, F.-Y.; Su, W.-F.; Huang, Y.-C. High-Performance Perovskite Solar Cells and Modules Fabricated by Slot-Die Coating with Nontoxic Solvents. *Nanomaterials* **2023**, *13*, 1760. [CrossRef]
69. Raptis, D.; Worsley, C.A.; Meroni, S.M.P.; Pockett, A.; Carnie, M.; Watson, T. Scalable Screen-Printed TiO_2 Compact Layers for Fully Printable Carbon-Based Perovskite Solar Cells. *Solar* **2022**, *2*, 293–304. [CrossRef]
70. Yang, Y.; Yuan, L.; Chang, Q.; Yang, Y.; Tang, X.; Wan, Z.; Du, J.; Wei, H.; Liu, C.; Guo, P.; et al. Cyclen molecule manipulation for efficient and stable perovskite solar cells. *J. Mater. Chem. A* **2024**, *12*, 13212–13218. [CrossRef]
71. Uddin, A.; Rana, P.J.S.; Ni, Z.; Yang, G.; Li, M.; Wang, M.; Gu, H.; Zhang, H.; Dou, B.D.; Huang, J. Iodide manipulation using zinc additives for efficient perovskite solar minimodules. *Nat. Commun.* **2024**, *15*, 1355. [CrossRef] [PubMed]
72. Wang, F.; Shi, X.; Yu, H.; Wang, L.; Ren, Z.; Chen, S. Efficient Blade-Coated p–i–n Perovskite Solar Cells and Modules Enabled by Effective Molecular N Doping. *Small* **2024**, *20*, 2306425. [CrossRef] [PubMed]
73. Gao, H.; Xiao, K.; Lin, R.; Zhao, S.; Wang, W.; Dayneko, S.; Duan, C.; Ji, C.; Sun, H.; Bui, A.D.; et al. Homogeneous crystallization and buried interface passivation for perovskite tandem solar modules. *Science* **2024**, *383*, 855–859. [CrossRef] [PubMed]
74. Sun, H.; Xiao, K.; Gao, H.; Duan, C.; Zhao, S.; Wen, J.; Wang, Y.; Lin, R.; Zheng, X.; Luo, H.; et al. Scalable Solution-Processed Hybrid Electron Transport Layers for Efficient All-Perovskite Tandem Solar Modules. *Adv. Mater.* **2023**, *36*, 2308706. [CrossRef] [PubMed]
75. Ren, Z.; Cui, Z.; Shi, X.; Wang, L.; Dou, Y.; Wang, F.; Lin, H.; Yan, H.; Chen, S. Poly(carbazole phosphonic acid) as a versatile hole-transporting material for p-i-n perovskite solar cells and modules. *Joule* **2023**, *7*, 2894–2904. [CrossRef]
76. Tutundzic, M.; Zhang, X.; Lammar, S.; Singh, S.; Marchezi, P.; Merckx, T.; Aguirre, A.; Moons, E.; Aernouts, T.; Kuang, Y.; et al. Toward Efficient and Fully Scalable Sputtered NiOx-Based Inverted Perovskite Solar Modules via Co-Ordinated Modification Strategies. *Sol. RRL* **2024**, *8*, 2300862. [CrossRef]
77. Xu, W.; Chen, B.; Zhang, Z.; Liu, Y.; Xian, Y.; Wang, X.; Shi, Z.; Gu, H.; Fei, C.; Li, N.; et al. Multifunctional entinostat enhances the mechanical robustness and efficiency of flexible perovskite solar cells and minimodules. *Nat. Photonics* **2024**, *18*, 379–387. [CrossRef]
78. Zhuang, J.; Liu, C.; Kang, B.; Cheng, H.; Xiao, M.; Li, L.; Yan, F. Rapid Surface Reconstruction in Air-Processed Perovskite Solar Cells by Blade Coating. *Adv. Mater.* **2023**, *36*, 2309869. [CrossRef]
79. Huang, C.; Tan, S.; Yu, B.; Li, Y.; Shi, J.; Wu, H.; Luo, Y.; Li, D.; Meng, Q. Meniscus-modulated blade coating enables high-quality α-phase formamidinium lead triiodide crystals and efficient perovskite minimodules. *Joule* **2024**, *8*, 2539–2553. [CrossRef]
80. Zhang, J.; Ji, X.; Wang, X.; Zhang, L.; Bi, L.; Su, Z.; Gao, X.; Zhang, W.; Shi, L.; Guan, G.; et al. Efficient and Stable Inverted Perovskite Solar Modules Enabled by Solid–Liquid Two-Step Film Formation. *Nano-Micro Lett.* **2024**, *16*, 190. [CrossRef]
81. Rana, P.J.; Febriansyah, B.; Koh, T.M.; Muhammad, B.T.; Salim, T.; Hooper, T.J.; Kanwat, A.; Ghosh, B.; Kajal, P.; Lew, J.H.; et al. Alkali additives enable efficient large area (>55 cm^2) slot-die coated perovskite solar modules. *Adv. Funct. Mater.* **2022**, *32*, 2113026. [CrossRef]
82. Sangale, S.S.; Kwon, S.; Patil, P.; Lee, H.; Na, S. Locally Supersaturated Inks for a Slot-Die Process to Enable Highly Efficient and Robust Perovskite Solar Cells. *Adv. Energy Mater.* **2023**, *13*, 2300537. [CrossRef]

83. Wang, L.; Zhang, T.; Yuan, S.; Qian, F.; Li, X.; Zheng, H.; Huang, J.; Li, S. Over 19% efficiency perovskite solar modules by simultaneously suppressing cation deprotonation and iodide oxidation. *ACS Appl. Mater. Interfaces* **2024**, *16*, 4751–4762. [CrossRef] [PubMed]
84. Subbiah, A.S.; Isikgor, F.H.; Howells, C.T.; Bastiani, M.D.; Liu, J.; Aydin, E.; Furlan, F.; Allen, T.G.; Xu, F.; Zhumagali, S.; et al. High-performance perovskite single-junction and textured perovskite/silicon tandem solar cells via slot-die-coating. *ACS Energy Lett.* **2020**, *5*, 3034–3040. [CrossRef]
85. Rana, P.J.; Febriansyah, B.; Koh, T.M.; Kanwat, A.; Xia, J.; Salim, T.; Hooper, T.J.; Kovalev, M.; Giovanni, D.; Aw, Y.C.; et al. Molecular Locking with All-Organic Surface Modifiers Enables Stable and Efficient Slot-Die-Coated Methyl-Ammonium-Free Perovskite Solar Modules. *Adv. Mater.* **2023**, *35*, 2210176. [CrossRef] [PubMed]
86. Li, J.; Dagar, J.; Shargaieva, O.; Maus, O.; Remec, M.; Emery, Q.; Khenkin, M.; Ulbrich, C.; Akhundova, F.; Márquez, J.A.; et al. Ink Design Enabling Slot-Die Coated Perovskite Solar Cells with >22% Power Conversion Efficiency, Micro-Modules, and 1 Year of Outdoor Performance Evaluation. *Adv. Energy Mater.* **2023**, *13*, 2203898. [CrossRef]
87. Worsley, C.A.; Dunlop, T.; Potts, S.J.; Bolton, R.; Jewell, E.; Watson, T. Infiltration Issues in Printed Mesoporous Perovskite Solar Cells: A Troubleshooting Guide. *J. Mater. Chem. C* **2024**, *12*, 9401–9411. [CrossRef]
88. Potts, S.J.; Bolton, R.; Dunlop, T.; Lacey, K.; Worsley, C.; Watson, T.; Jewell, E. Enhancing the Performance of the Mesoporous TiO_2 Film in Printed Perovskite Photovoltaics through High-Speed Imaging and Ink Rheology Techniques. *Adv. Funct. Mater.* **2024**, *34*, 2401959. [CrossRef]
89. Srisamran, N.; Sudchanham, J.; Sriprachuabwong, C.; Srisawad, K.; Pakawatpanurut, P.; Lohawet, K.; Kumnorkaew, P.; Krajangsang, T.; Tuantranont, A. Enhanced performance and stability of fully printed perovskite solar cells and modules by ternary additives under high humidity. *Energy Fuels* **2023**, *37*, 6049–6061. [CrossRef]
90. Li, F.; Lin, F.R.; Jen, A.K.-Y. Current state and future perspectives of printable organic and perovskite solar cells. *Adv. Mater.* **2024**, *36*, 2307161. [CrossRef]
91. Di Giacomo, F.; Shanmugam, S.; Fledderus, H.; Bruijnaers, B.J.; Verhees, W.J.; Dorenkamper, M.S.; Veenstra, S.C.; Qiu, W.; Gehlhaar, R.; Merckx, T.; et al. Up-scalable sheet-to-sheet production of high efficiency perovskite module and solar cells on 6-in. substrate using slot die coating. *Sol. Energy Mater. Sol. Cells* **2018**, *181*, 53–59. [CrossRef]
92. Nia, N.Y.; Giordano, F.; Zendehdel, M.; Cinà, L.; Palma, A.L.; Medaglia, P.G.; Zakeeruddin, S.M.; Grätzel, M.; Di Carlo, A. Solution-based heteroepitaxial growth of stable mixed cation/anion hybrid perovskite thin film under ambient condition via a scalable crystal engineering approach. *Nano Energy* **2020**, *69*, 104441.
93. Chalkias, D.A.; Mourtzikou, A.; Katsagounos, G.; Kalarakis, A.N.; Stathatos, E. Development of Greener and Stable Inkjet-Printable Perovskite Precursor Inks for All-Printed Annealing-Free Perovskite Solar Mini-Modules Manufacturing. *Small Methods* **2023**, *7*, 2300664. [CrossRef] [PubMed]
94. Calabrò, E.; Matteocci, F.; Palma, A.L.; Vesce, L.; Taheri, B.; Carlini, L.; Pis, I.; Nappini, S.; Dagar, J.; Battocchio, C.; et al. Low temperature, solution-processed perovskite solar cells and modules with an aperture area efficiency of 11%. *Sol. Energy Mater. Sol. Cells* **2018**, *185*, 136–144. [CrossRef]
95. Bu, T.; Liu, X.; Li, J.; Huang, W.; Wu, Z.; Huang, F.; Cheng, Y.B.; Zhong, J. Dynamic antisolvent engineering for spin coating of 10×10 cm^2 perovskite solar module approaching 18%. *Sol. RRL* **2020**, *4*, 1900263. [CrossRef]
96. Bu, T.; Li, J.; Zheng, F.; Chen, W.; Wen, X.; Ku, Z.; Peng, Y.; Zhong, J.; Cheng, Y.-B.; Huang, F. Universal passivation strategy to slot-die printed SnO_2 for hysteresis-free efficient flexible perovskite solar module. *Nat. Commun.* **2018**, *9*, 4609. [CrossRef] [PubMed]
97. Xiao, K.; Lin, Y.-H.; Zhang, M.; Oliver, R.D.J.; Wang, X.; Liu, Z.; Luo, X.; Li, J.; Lai, D.; Luo, H.; et al. Scalable processing for realizing 21.7%-efficient all-perovskite tandem solar modules. *Science* **2022**, *376*, 762–767. [CrossRef] [PubMed]
98. Yang, Z.; Zhang, W.; Wu, S.; Zhu, H.; Liu, Z.; Liu, Z.; Jiang, Z.; Chen, R.; Zhou, J.; Lu, Q.; et al. Slot-die coating large-area formamidinium-cesium perovskite film for efficient and stable parallel solar module. *Sci. Adv.* **2021**, *7*, eabg3749. [CrossRef]
99. Hamidon, M.N.; Farnana, T.D.; Hasan, I.H.; Sali, A.; Isa, M.M. Printing of passive RFID tag antennas on flexible substrates for long read distance applications: Materials and techniques. *J. Sci. Adv. Mater. Devices* **2024**, *9*, 100778. [CrossRef]
100. Ma, Y.; Liu, C.; Zhang, M.; Mai, Y. Review on the effects of solvent physical properties on the performance of slot-die coated perovskite solar cells. *Surf. Sci. Technol.* **2024**, *2*, 25. [CrossRef]
101. Cheng, J.; Liu, F.; Tang, Z.; Li, Y. Scalable Blade Coating: A Technique Accelerating the Commercialization of Perovskite-Based Photovoltaics. *Energy Technol.* **2021**, *9*, 2100204. [CrossRef]
102. Kirk, B.P.; Bjuggren, J.M.; Andersson, G.G.; Dastoor, P.; Andersson, M.R. Printing and Coating Techniques for Scalable Organic Photovoltaic Fabrication. *Materials* **2024**, *17*, 2511. [CrossRef] [PubMed]